Naval Research Laboratory

Washington, DC 20375-5320

A Numerical Model for the Development of a Boundary Layer Diffusion Flame Over a Porous Flat Plate

RAMAGOPAL ANANTH
PATRICIA A. TATEM

Navy Technology Center for Safety and Survivability
Chemistry Division

CHUKA C. NDUBIZU

GEO-CENTERS, Inc.
4640 Forbes Blvd., Suite 130
Lanham, MD

April 23, 2001

20010509 070

REPORT DOCUMENTATION PAGE

1. AGENCY USE ONLY (Leave Blank)	2. REPORT DATE April 23, 2001	3. REPORT TYPE AND DATES COVERED

4. TITLE AND SUBTITLE

A Numerical Model for the Development of a Boundary Layer Diffusion Flame Over a Porous Flat Plate

5. FUNDING NUMBERS

6. AUTHOR(S)

Ramagopal Ananth, Chuka C. Ndubizu,* and Patricia A. Tatem

7. PERFORMING ORGANIZATION NAME(S) AND ADDRESS(ES)

Naval Research Laboratory
Washington, DC 20375-5320

8. PERFORMING ORGANIZATION REPORT NUMBER

NRL/MR/6183--01-8547

9. SPONSORING/MONITORING AGENCY NAME(S) AND ADDRESS(ES)

Office of Naval Research (ONR 822)
800 North Quincy Street
Arlington, VA 22217-5660

10. SPONSORING/MONITORING AGENCY REPORT NUMBER

11. SUPPLEMENTARY NOTES

*GEO-CENTERS, Inc., 4640 Forbes Blvd., Suite 130, Lanham, MD 20706

12a. DISTRIBUTION/AVAILABILITY STATEMENT

Approved for public release; distribution is unlimited.

12b. DISTRIBUTION CODE

13. ABSTRACT (Maximum 200 words)

Time-dependent solutions of full Navier-Stokes equations were obtained for gas phase combustion over a porous plate burner using Barely Implicit Flux Corrected Transport (BIC-FCT) algorithms. Unlike the previous boundary layer studies, our solutions are valid near the leading edge as well as the downstream. The simulations show formation of a triple flame structure, upon ignition near the leading edge. The triple flame gets weaker with time as it spreads across the porous plate and finally transitions to a typical boundary layer structure at steady state. The steady state solutions predict a maximum in axial velocity with distance from the solid surface and are similar to the existing experimental observations. The heat feedback from the flame to the surface shows a steep increase near the leading edge followed by a relatively slow decrease with distance from the leading edge. Away from the leading edge, the heat flux profile may be fitted by a power law. This is in sharp contrast to the existing boundary layer theories that show a monotonic decrease in the heat feedback. The results show that 70% of the total heat feedback occurs close (within 3 cm) to the leading edge.

14. SUBJECT TERMS		15. NUMBER OF PAGES 67
CFD modeling Gas phase combustion	Barely Implicit Flux Corrected Transport Boundary layer theory	16. PRICE CODE

17. SECURITY CLASSIFICATION OF REPORT UNCLASSIFIED	18. SECURITY CLASSIFICATION OF THIS PAGE UNCLASSIFIED	19. SECURITY CLASSIFICATION OF ABSTRACT UNCLASSIFIED	20. LIMITATION OF ABSTRACT UL

CONTENTS

NOMENCLATURE

Text

A	Coeifficient in Arrhenius rate expression, $(\#molecules/cm^3)^{-(m+n-1)}\ sec^{-1}$
Av	Avgadro number, #molecules/gmole
$a1_k.a4_k$	Fitted coefficients in polynomial expression for specific enthalpy, hk, of specie k
$b1_{kl}$	Fitted coefficients in power law expression for diffusivity, D_{kl}, of a binary mixture containing species k and l
$b2_{kl}$	Fitted coefficients in power law expression for diffusivity, D_{kl}, of a binary mixture containing species k and l
C_k	Number density of the specie, k, $\#molecules/cm^3$
$c1_k$	Fitted coefficients in power law expression for viscosity, μ_k, of specie k
$c2_k$	Fitted coefficients in power law expression for viscosity, μ_k, of specie k
D_{kl}	Diffusion coefficient of specie k in a binary mixture of species k and l, cm^2/sec
D_{km}	Diffusivity of specie k in a gas mixture, cm^2/sec
$d1_k$	Fitted coefficients in power law expression for thermal conductivity, λ_k, of specie k
$d2_k$	Fitted coefficients in power law expression for thermal conductivity, λ_k, of specie k
E	Total energy density of gas mixture, $ergs/cm^3$
E_a	Reaction activation energy, ergs/gmole
e	Specific energy of gas mixture, ergs/gm
H	Height of the channel, cm
HRR_v	Enerrgy release rate per unit volume, $ergs/cm^3 sec$
h_k	Specific enthalpy of specie k, ergs/gmole
h_w	Surface heat transfer coefficient, $ergs/cm^2.sec.K$
K_k	Fitted coefficients in polynomial expression for radiation extinction coefficient of specie k
K_{pk}	Gray body radiation extinction coefficieent of specie k=CO_2, H_2O
K_{pm}	Gray body radiation extinction coefficieent of gas mixture
k_c	Pseudo first-order kinetic rate constant, sec^{-1}
L	Total length of the plate, $L=L_1+L_2+L_3$, cm
$L_{1,2,3}$	Lengths of the leading non-porous section 1, porous plate section 2, and post-flame, non-porous section 3 respectively, cm
M_k	Molecular weight of specie k, gm/gmole
m,n	Constants in the expression for psuedo first order rate constant
P	Pressure, $dynes/cm^2$
Q_b	% of area integrated heat feed back from the flame to the surface
Q_r	Radiative heat loss from the gas phase, $ergs/cm^3 sec$
q_i	Heat flux in direction i, $ergs/cm^2 sec$
q_w	Heat flux at the solid surface, $ergs/cm^2 sec$
R	Universal gas constant, 8.3144e07 ergs/gmole.K
s	# of carbons in the fuel (normal hydrocarbon, aliphatic)
T	Temperature, K

t	Time, sec
U_{dk}	Diffusion velocity for specie k in x-direction, cm/sec
u	Axial gas velocity in x-direction, cm/sec
V_{dk}	Diffusion velocity for specie k in y-direction, cm/sec
v	Vertical gas velocity in y-direction, cm/sec
W_k	Rate of consumption or production of specie k due to reaction, #molecules/cm^{3}sec
X_k	Mole fraction of specie k
x	Axial distance from the leading edge of the leading non-porous section 1, cm
Y_k	Mass fraction of specie k
y	Vertical distance from the solid surface, cm

Greek Symbols

ΔH_c	Heat of combustion, ergs/gmole
τ_{ij}	Stress tensor, dynes/cm^2
λ_k	Thermal conductivity of specie k, ergs/cm.sec.K
λ_m	Thermal conductivity of gas mixture, ergs/cm.sec.K
μ_k	Kinematic viscosity of specie k
μ_m	Kinematic viscosity of gas mixture
ρ	Gas density, gm/cm^3
ϕ_{kj}	Dimensionless mixture property in the expression for mixture viscosity, μ_m

Subscripts

c	Combustion
d	Diffusion
i	Index in x-direction, i=1,...,nx
j	Index in y-direction, j=1,..., ny
k	Specie index, k=1,.., 5
l	Specie index, l=1,.., 5
m	Gas mixture
p	Gray body radiation
r	Radiation
w	At the surface

A NUMERICAL MODEL FOR THE DEVELOPMENT OF A BOUNDARY LAYER DIFFUSION FLAME OVER A POROUS FLAT PLATE

1.0 INTRODUCTION

A large fire often goes through different phases; ignition, flame spread across the fuel surface, fully involved "steady-burning", fire decay, extinction, and product cool-off. Maximum heat release is often observed during the fully involved burning of a material and can be reproduced in the laboratory by air flow past a flat plate, which is ignited along the entire surface. This forms a boundary layer flame over the solid plate. The heat feedback from the flame drives the pyrolysis of the solid and generates fuel vapor, which ejects from the surface and diffuses into the bulk of the combusting gas. Suppression or extinction of the flame can be achieved by introducing fine water droplets with air. Our ultimate goal is to understand the fundamental mechanisms of suppression of the boundary layer flame by developing a numerical model as described by Ananth et al. (1999, 2000) and by performing laboratory experiments. As a first step toward this goal, we have developed a gas phase submodel for a boundary layer flame over a porous plate through which a fuel gas (n-pentane) is injected at a known rate in order to simulate the fuel surface. This report documents the details of the numerical development for the gas phase submodel and its predictions of the boundary layer flame structure, flame standoff distance, heat feedback, and mass transport at the surface. This is a fully time-dependent model that describes the flame development from the point of ignition to a steady flame covering the entire plate. Modeling unsteady state is crucial for future studies of suppression/extinction, which are intrinsically transient phenomena. Furthermore, the solutions are given for the entire surface of the porous plate including the leading edge, which receives the highest degree of heat feedback from the flame and could play a crucial role in suppression of the flame. Unlike the model presented in this report, existing theories for the porous burner assume steady state and focused mainly far downstream of the leading edge rather than the entire plate. In the future, we will replace the porous plate with a pyrolyzing solid by adding pyrolysis submodels to study suppression by water mist.

Studies using a porous plate burner are of interest in their own right because they are well suited for fundamental study of boundary layer flames. They provide a well defined solid boundary unencumbered by the complex and poorly explored phenomena of solid pyrolysis, phase change, and moving boundary effects. Indeed, the complex nature of pyrolysis has eluded a detailed comparison of theory and experiments for temperature, velocity, and regression rate profiles for boundary layer flames to date. This is especially a problem as one approaches the leading edge, where most pyrolysis takes place resulting in large distortions of the interface with time. Theories of PMMA (Poly methyl methacrylate or "plexi-glass") combustion ignore the moving boundary effects and the complex nature of pyrolysis. Furthermore, in their studies of PMMA combustion, Kodama et al. (1987) noted that even the gas phase combustion is not well defined, and Chen and Tien (1986) used simple hydrocarbon chemistry, such as methane, instead of the monomer (methyl methacrylate). The boundary layer flames formed over a porous plate,

---

however, use simple hydrocarbon fuels with well defined kinetics, and capture the main features of fluid dynamic, heat transfer and combustion characteristics as those flames formed over pyrolyzing solids. The heat and mass transfer in the gas and on the porous surface still remain coupled and are set by the injection rate. However, the injection rate can be varied independent of the heat feedback to the surface unlike PMMA combustion, where they are coupled. Also, the injection rate of fuel is set uniform along the plate in the experiments performed on porous plate burners in the literature. The uniform injection of fuel results in significant variation in surface temperature and specie concentrations along the plate, unlike the case of PMMA surface, where the surface conditions are dictated by the complex physics and chemistry of pyrolysis and may remain relatively uniform. Therefore, boundary layer combustion over a porous plate burner is significantly different from a pyrolyzing surface, and have both theoretical and experimental advantages. Combustion over a porous plate burner could give fundamental insights into reactive boundary layers and their suppression by enabling definitive comparisons between experiments and theories for the entire surface including the leading edge.

Yet, studies of stationary gaseous flames over a porous plate are limited as opposed to the large number of studies which exist for flame spread, and to a lesser extent stationary flames, over a condensed fuel. Most studies of the gas phase combustion problem over a porous plate neglect streamwise diffusion and make boundary layer approximations. A complete understanding of the problem, which includes both the leading edge and the downstream boundary layer, is lacking as discussed below. A complete solution of full Navier-Stokes equations for density, velocity components, specie concentrations, temperature, heat release rate have not been quantitatively explained in detail in the literature. The velocity profiles are very complex and have not been fully understood. Especially unclear is the complex nature of coupling between gas and solid phases, which determine the surface temperature, concentration of species and heat feedback. The exact relationship among mass injection rate, heat loss through the porous plate, surface temperature, surface concentration of species, and heat feedback have not been determined quantitatively, even for a porous plate burner. It is also not clear to what extent the surface conditions affect the flame characteristics and vice-a-versa. Such an understanding of surface-flame interactions is crucial for gaining insights into the role of solid phase phenomena in the combustion of solids.

2.0   LITERATURE REVIEW

Emmons (1956) obtained similarity solutions to forced-flow boundary layer equations using flame sheet approximation to eliminate the reaction terms from the equations. He assumed infinite rate kinetics (flame sheet model) and constant Prandtl, Pr, Schmidt, Sc, and Lewis, Le. He decoupled the gas phase from the liquid phase by assuming constant wall temperature and fuel mass fraction, as discussed by Pagni (1980), rather than calculating them from vapor-liquid equilibrium. He showed explicitly that the rate of heat feedback decreased as the square root of the distance from the leading edge. However, his solutions are valid for a non-uniform rate of fuel ejection from the surface rather than uniform injection rates employed in porous plate burners. Furthermore, solutions of boundary layer equations do not include streamwise diffusion terms and neglect y-momentum. Therefore, the solutions are valid only at large distances from the leading edge of the porous plate. Indeed, when extrapolated to the leading edge, the

boundary layer solutions result in infinite rate of heat feedback due to the singularity. This is a crucial shortcoming because heat feedback is largest, but finite, near the leading edge, where the flame is closest to the surface. In this work, we will obtain numerical solutions of full Navier-Stokes equations that are valid over the entire plate. We will show that most of the heat feedback to the surface occur in the neighborhood of the leading edge. Heat release rate and expansion flow, which occurs due to the release of combustion energy, are expected to be largest near the leading edge and are not accounted for in the boundary layer solutions. We consider finite rate kinetics and the effects of variable properties.

Kikkawa and Yoshikawa (1973) generalized Emmons solutions of boundary layer equations (without the axial diffusion terms and without y-momentum) to uniform injection rates along a porous plate burner, finite rate kinetics, variable specie concentrations at the surface, and variable physical properties of the gas. They also included mass transfer coupling at the surface by requiring that the mass injection rate of the fuel be equal to the sum of diffusive and convective fluxes ejecting from the surface. They showed that the gas properties vary significantly across the boundary layer (especially Le, which can vary from below 1 to above 1 and by a factor of 3) for combustion of propane. They also showed, for the first time, that the variation in properties due to gas composition alone could decrease the maximum flame temperature by 700 C and the flame standoff distance by about 20%. Surprisingly, this finite rate, Arrhenius model seems to result in only 100 C lower than the infinite rate model for the maximum flame temperature and in very little change in flame standoff distance. They also showed that the fuel concentration and temperature vary significantly along the surface of the porous plate for uniform injection rate of propane. This is unlike liquid methanol calculations, which showed uniform temperature and fuel distribution at the surface due to decreasing rate of vaporization along the surface of the burner. The presence of a non-porous leading plate in front of the porous plate was shown to increase the flame standoff distance especially near the leading edge of the porous plate section. The leading plate reduces the velocity of air approaching the flame due to no-slip at the surface. The variable density with temperature seems to create an inflection point in the axial velocity profile, when compared to the corresponding similarity solutions for boundary layers with fixed density. Anderotte and Petraci (1981) resolved the problem posed by Kikkawa and Yoshikawa (1973) using specie diffusivity equal to the diffusivity of fuel in nitrogen, but independent of composition of the local gas mixture. Use of fuel diffusivity in place of the diffusivity of the local gas mixture appears to have lead to good agreement with the results of Kikkawa and Yoshikawa (1973) for the gas temperature and elemental mass fractions. However, these calculations were performed for a liquid fuel, where the fuel ejection rates from the surface are non-uniform. It may also hold true for uniform injection of a gas fuel at small injection rate, however, this has not been shown.

Hirano and Kanno (1973) performed experiments with propane and methane gases injected uniformly through a porous plate. They have made detailed measurements of both the axial fluid velocity and temperature profiles across the boundary layer. They observed a maximum in the axial velocity of the fluid with distance from the solid surface ("velocity overshoot"). Anderotte, Andreussi, and Petraci (1984) also observed the maximum in axial velocity for liquid fuels and showed that the maximum value decreases with increased air velocity. The boundary layer solutions given by Emmons (1956), Kikkawa and Yoshikawa (1973), and Anderotte and Petraci (1981) predict a monotonic axial velocity profile with distance from the

3

burner surface contrary to the experimental observations of Hirano and Kanno (1973). They assume uniform axial velocity and zero axial pressure gradient outside the boundary layer. The density variation with temperature lead to an inflection point in the axial velocity profile rather than a maximum with distance from the burner surface. Levid and Berlad (1976) considered the effect of gravity on the boundary layer flame. However, their results underpredict the observed maximum in axial velocity with distance from the surface significantly. Ramachandran and Raghunandan (1983,1984) also made detailed measurements of temperature and velocity profiles and observed a maximum in axial velocity profile for n-pentane combustion in a confined channel. Ramachandran and Raghunandan (1984) also generalized solutions of Kikkawa and Yoshikawa (1973) to include the axial pressure gradient term in the equation for the x-momentum. The predictions show a maximum in the axial velocity profile, and they were in reasonable agreement with their data on n-pentane at large distances from the leading edge of the porous plate. The maximum in the axial velocity appears to have resulted due to acceleration of flow near the center of the channel to compensate for the reduced flow in the boundary layers near the lower and upper wall of the channel. Therefore, when the upper wall of the channel was removed (unconfined flow), the maximum in the axial velocity could not be predicted because pressure does not change with axial distance. The gas temperatures were, however, over predicted by the their theory. This may be because Ramachandra and Raghunandan (1984) used flame sheet approximation with infinite kinetics, specie independent transport properties, where Pr=Sc and Le=1, unlike the work of Kikkawa and Yoshikawa (1973). Furthermore, the flame standoff distance and axial fluid velocity are calculated to vary significantly with injection velocity, while the data showed a relatively weak dependence. The surface concentrations of species are calculated from mass balance and are predicted to quickly reach an asymptotic value with distance. However, no measurements were available for the surface concentrations to explain the maximum in the axial velocity with distance from the burner surface.

As mentioned previously, boundary layer solutions do not apply near the leading edge and full Navier-Stokes equations must be considered to explain fully the measured temperature and velocity profiles. Chen and Tien (1986) obtained steady-state solutions of full Navier-Stokes equations to study flame stabilization in the neighborhood (< 3 cm) of the leading edge. They considered forced convection and included both streamwise diffusion and y-momentum near the leading edge. Chen and Tien (1986) concluded that a much longer (> 3 cm) length of the plate should be considered to realize the boundary layer limit in addition to the leading edge limit. Mao, Kodama, and Fernadez-Pello (1984) and Kodama, Miyasaka and Fernandez-Pello (1987) also obtained steady-state solutions of full Navier-Stokes equations for the combustion of PMMA and n-heptane for plate lengths of 5 cm. They considerd mixed convection (forced convection and gravity) and the effects of oxygen concentration in air on flame stability and extinction limits. These solutions (Chen and Tien (1986), Mao, et al. (1984), and Kodama et al. (1987)) showed that the incoming air flow was diverted upward near the leading edge of the flame due to thermal expansion. The thermal expansion near the leading edge manifested into a maximum in axial velocity profile at an axial distance downstream of the leading edge. Even though these works provided detailed discussions of the leading edge, their solutions do not apply quantitatively for a porous plate burner since they consider non-uniform ejection rates of fuel from the surface. Furthermore, unlike the porous plate gas-burner, definitive comparisons with experimental data could not be made due to poorly defined pyrolysis processes of PMMA, not well-defined

4

combustion kinetics, and the moving boundary effect, which is especially significant near the leading edge. Ha et al. (1991) obtained steady-state solutions of full Navier-Stokes equations for the combustion of hydrogen injected uniformly through the porous burner. They focused mainly on the axial velocities and did not provide a comprehensive discussion of the entire solution. Their solutions also show a maximum in axial velocity profile due to thermal expansion near the leading edge and are in good agreement with their experimental data. This is contrary to the results of Ramachandra and Raghunandan (1984), who considered the effects of an upper wall and neglected the effects near the leading edge. Recently, microgravity experiments were performed by Brahmi et al. (1999) for a porous plate burner at low velocities of air (less than 10 cm/sec) and measured flame standoff distance for ethane combustion.

All of the theoretical studies mentioned above assume steady state and are not suitable for describing fully flame stability, suppression, and extinction. Even at steady state, a detailed understanding of the solutions is lacking for the entire surface, which includes both the leading edge and the boundary layer limits. The velocity profiles are affected by various phenomena, such as no slip at the wall, gas expansion near the leading edge, cross-flow of air and fuel, inlet velocity profile, and the presence of a leading section preceding the porous plate. The relative importance and the intricate interactions among these effects remain unclear. Furthermore, a detailed comparisons of the profiles with precise experimental data are critical for a full understanding and are not available. In this work, we will obtain time-dependent solutions of full-Navier-Stokes equations for a flame formed over a porous plate for n-pentane combustion for the first time. Since they include axial diffusion terms, y-momentum, and finite rate combustion kinetics, they are valid over the entire surface of the porous plate, which extends several centimeters in length. We will describe the dynamics of flame development across the solid surface from the time of ignition at the leading edge. We will provide a comprehensive and full discussion of steady-state solutions for temperature, heat release rate, density, pressure, axial and vertical velocities and specie concentrations. We will also describe the coupling among the variables at the surface and their variation with distance along the surface. We will include the effects of heat transport into the burner as a boundary condition rather than the constant wall temperature used in previous works. Specifically, we will show that heat feedback, specie concentration and temperature variation along the surface are different from the existing theories for a porous plate burner. Furthermore, we will show that most heat feedback occurs within the first two-centimeter distance from the leading edge.

3.0 ANALYSIS

We consider air flow past a solid surface, which consists of a leading impermeable section of length L_1, followed by a porous section of length L_2, and a trailing impermeable section of length L_3, as shown in Figure 1. The leading section establishes no-slip condition and sets up a momentum boundary layer before the air stream approaches the leading edge of the porous plate through which fuel gas is injected uniformly at a fixed mass flow rate. The flow over the solid is assumed to be two dimensional. The length in the third dimension is assumed to be much larger than the boundary layer thickness so that the gradients in that direction become negligible. The forced convection is assumed to dominate the gravity effects, which are neglected in the analysis.

5

11x19 cm

150x200 stretched cells

air,u_0 cm/sec

flame

non porous section 3

L_3=10 cm

porous section 2

fuel injection

v_w=0.3 cm/sec

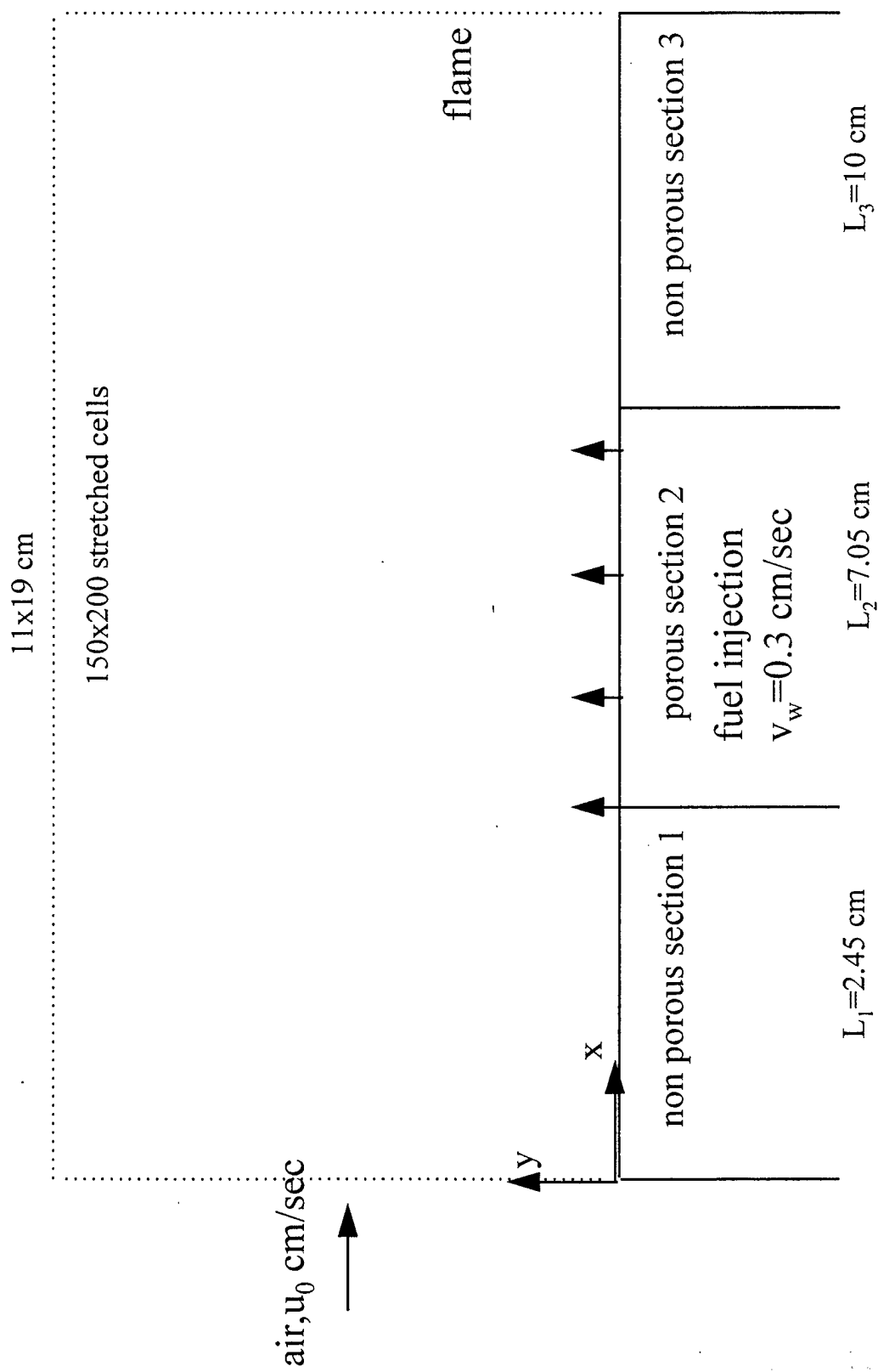L_2=7.05 cm

non porous section 1

L_1=2.45 cm

x

y

Figure 1   Schematic of the computational domain

Radiative heat loss from hot gases to the ambient is included. However, under the forced convection conditions, radiative transport of heat between the fuel surface and hot gases is not included. Also, the radiative heat loss from the fuel surface to the ambient is not included. The gas injected through the porous surface is assumed to be pure fuel with uniform and pre-specified mass injection rate. All physical properties are functions of temperature and composition. Therefore, Pr, Sc and Le are functions of both temperature and composition. The gas phase is assumed to obey the ideal gas law and density is an unknown.

The entire burner surface is treated as non-catalytic and inert. The porous section of the burner is assumed to be semi-permeable to fuel gas and does not allow mass transport from the gas phase into the burner. The heat loss through the porous section of the burner is assumed to be proportional to the temperature difference between the surface and ambient, following Newton's law of cooling with a heat transfer coefficient, h_w. Therefore, temperature and specie concentrations at the surface vary along the porous surface and are unknowns.

Fuel gas mixes with the approaching air stream in a cross-flow configuration by diffusion and convection. Heat is added for a period of 10 milliseconds at a fixed rate to several cells just above the leading edge of the plate to ignite the gases. Upon ignition at the leading edge, a diffusion flame spreads across the gas above the plate and forms a boundary layer flame at steady state. Time-dependent Navier-Stokes equations describe the development of a laminar flame across the surface from the ignition source. The equations are written in x and y co-ordinates with the origin located at the beginning of the leading plate.

Continuity

$$\frac{\partial \rho}{\partial t} + \frac{\partial \rho u}{\partial x} + \frac{\partial \rho v}{\partial y} = 0, \qquad (1)$$

x-momentum

$$\frac{\partial u}{\partial t} + \frac{\partial \rho u^2}{\partial x} + \frac{\partial \rho u v}{\partial y} = -\frac{\partial P}{\partial x} + \frac{\partial \tau_{xx}}{\partial x} + \frac{\partial \tau_{yx}}{\partial y}, \qquad (2)$$

y-momentum

$$\frac{\partial v}{\partial t} + \frac{\partial \rho u v}{\partial x} + \frac{\partial \rho u^2}{\partial y} = -\frac{\partial P}{\partial y} + \frac{\partial \tau_{xy}}{\partial x} + \frac{\partial \tau_{yy}}{\partial y}, \qquad (3)$$

energy

$$\frac{\partial E}{\partial t} + \frac{\partial u(E+P)}{\partial x} + \frac{\partial v(E+P)}{\partial y} = \frac{\partial u\tau_{xx}}{\partial x} + \frac{\partial u\tau_{xy}}{\partial y} + \frac{\partial v\tau_{yx}}{\partial x} + \frac{\partial v\tau_{yy}}{\partial y}$$

$$+ \frac{\partial q_x}{\partial x} + \frac{\partial q_y}{\partial y} + \frac{W_k \Delta H_c}{Av} + Q_r , \qquad (4)$$

specie,k, conservation

$$\frac{\partial C_k}{\partial t} + \frac{\partial u C_k}{\partial x} + \frac{\partial v C_k}{\partial y} = \frac{\partial U_{dk} C_k}{\partial x} + \frac{\partial V_{dk} C_k}{\partial y} + W_k , \qquad (5)$$

where ρ is the gas density. The quantities u and v are axial and vertical velocity components in x and y directions respectively. Here, P is pressure, E is total energy density, and C_k are specie number densities. The first term on left-hand side of equations (1-5) represents the transient effects, second and third terms represent convection in x and y directions respectively. The first term on the right-hand side of the momentum equations (2) and (3) represent pressure gradients. The second and third terms represent momentum diffusion. The first to fourth terms on the right-hand side of energy equation (4) represent work, fifth and sixth terms represent thermal diffusion, seventh term represents heat released due to combustion, and the last term represents radiative heat loss to the ambient. The first and second terms of the right-hand side of specie equation (5) represent mass diffusion, where U_{dk} and V_{dk} are diffusion velocities in x and y directions respectively. The last term on the right-hand side represents consumption or generation of specie k due to the combustion reaction.

3.1 Transport Fluxes

The viscosity μ effects are contained in shear stress τ, which relates to velocity gradients by the following equations,

$$\tau_{xx} = \mu_m \left(\frac{4}{3}\frac{\partial u}{\partial x} - \frac{2}{3}\frac{\partial v}{\partial y} \right) , \qquad (6)$$

$$\tau_{xy} = \tau_{yx} = \mu_m \left(\frac{\partial u}{\partial y} + \frac{\partial v}{\partial x} \right) , \qquad (7)$$

and

8

$$\tau_{yy} = \mu_m \left(\frac{4}{3}\frac{\partial v}{\partial y} - \frac{2}{3}\frac{\partial u}{\partial x} \right) . \qquad (8)$$

The conductive fluxes q depend on gas conductivity λ and temperature gradients, and are given by

$$q_x = -\lambda_m \frac{\partial T}{\partial x} + \sum_{k=1}^{N} (h_k C_k U_{dk}) / Av , \qquad (9)$$

and

$$q_y = -\lambda_m \frac{\partial T}{\partial y} + \sum_{k=1}^{N} (h_k C_k V_{dk}) / Av . \qquad (10)$$

The first term in equations (9) and (10) represent thermal conduction , the second term represents Defour effects, where h_k is specific enthalpy of specie k, Av is Avagadro number, λ is gas conductivity, and T is gas temperature. The diffusive fluxes in x and y directions are U_{dk} and V_{dk} respectively and are given by

$$_{dk} = -\frac{1}{X_k} D_{km} \frac{\partial X_k}{\partial x} + \sum_{k=1}^{N} \frac{Y_k}{X_k} D_{km} \frac{\partial X_k}{\partial x} , \quad k = 1,2,...N , \qquad (11)$$

and

$$V_{dk} = -\frac{1}{X_k} D_{km} \frac{\partial X_k}{\partial y} + \sum_{k=1}^{N} \frac{Y_k}{X_k} D_{km} \frac{\partial X_k}{\partial y} , \quad k = 1,2,...N , \qquad (12)$$

where, X_k and Y_k are mole and mass fractions of specie k respectively, D_{km} are equivalent binary diffusivities of specie k in the gas mixture. The gas mixture contains N number of components.

3.2 Thermodynamic Equations of State

Equations of state further define the total energy density E and specific internal energy e, and specific enthalpy h_k as

$$E = \rho e + \frac{1}{2}\rho(u^2 + v^2), \qquad (13)$$

$$\rho e = \sum_{k=1}^{N} \frac{C_k h_k}{Av} - P, \qquad (14)$$

and

$$h_k = a1_k + a2_k T + a3_k T^2 + a4_k T^3, \ k = 1,2,\ldots N, \qquad (15)$$

where $a1_k \ldots, a4_k$ are polynomial coefficients for specie k and are taken from sources such as those compiled by NIST (www.nist.gov), University of Berkeley (www.ucb.edu), and Penner (1957). The ideal gas law is

$$P = RT \sum_{k=1}^{N} \frac{C_k}{Av}, \qquad (16)$$

the mass specific heats, C_{pk}, of specie k are

$$C_{pk} = \frac{1}{M_k}\frac{\partial h_k{'}}{\partial T}, \ k = 1,2,\ldots N, \qquad (17)$$

and the mass specific heat of the gas mixture, C_{pm}, is

$$C_{pm} = \sum_{k=1}^{N} Y_k C_{pk}. \qquad (18)$$

3.3   Transport Properties

The transport properties are calculated from kinetic theory of gases described by Chapman-Enskog equations. The diffusivities of specie k in a mixture D_{km} are calculated from binary diffusion coefficients D_{ij} and mixture composition using

$$D_{km} = \frac{1-Y_k}{\displaystyle\sum_{l=1,l\neq k}^{N} \frac{X_l}{D_{kl}}}, \ k = 1,2,\ldots N, \qquad (19)$$

where the binary diffusion coefficients are related to temperature by fitting a power law in the range of 300 to 3000 K to evaluate $b1_{ij}$ and $b2_{ij}$:

$$D_{kl} = b1_{kl} T^{b2_{kl}} \Big/ \sum_{k=1}^{N} C_k \;, \quad k = 1,2,\ldots N \;. \tag{20}$$

The mixture viscosity is calculated from specie viscosities μ_k and mixture composition Y_k from the following equations

$$\mu_m = \sum_{k=1}^{N} \frac{Y_k \mu_k}{\sum_{j=1}^{N} Y_j \phi_{kj}} \;, \tag{21}$$

where

$$\phi_{kj} = \frac{1}{\sqrt{8}} \left(1 + \frac{M_k}{M_j}\right)^{-\frac{1}{2}} \left(1 + \left(\frac{\mu_k}{\mu_j}\right)^{\frac{1}{2}} \left(\frac{M_j}{M_k}\right)^{\frac{1}{4}}\right)^2 \;. \tag{22}$$

The specie viscosities are related to temperature by a power law given by

$$\mu_k = c1_k T^{c2_k} \;, \quad k = 1,2,\ldots N \;, \tag{23}$$

where $c1_k$ and $c2_k$ are known constants. Mixture conductivities, λ_m, which depend on the individual conductivities of the species and mixture composition and are given by

$$\lambda_m = \frac{1}{2} \left(\sum_{k=1}^{N} Y_k \lambda_k + \frac{1}{\sum_{k=1}^{N} \dfrac{Y_k}{\lambda_k}} \right) \;. \tag{24}$$

The specie conductivities are also related to temperature by a power law

$$\lambda_k = d1_k T^{d2_k} \;, \quad k = 1,2,\ldots N \;, \tag{25}$$

where $d1_k$ and $d2_k$, are known constants. Eucken equation is used for the conductivity of H_2O vapor. Therefore, all the transport properties are functions of both the temperature and composition.

3.4 Radiative Loss

Heat loss, Q_r, from the hot gases to the ambient is assumed to follow Stefan-Boltzman law and is

11

$$Q_r = K_{pm}\sigma\left(T^4 - T_\infty^4\right) . \qquad (26)$$

The gray body extinction coefficient, K_{pm}, is calculated based on the concentrations of carbon dioxide and water using
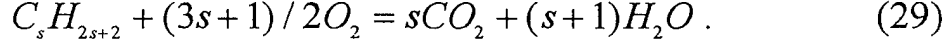
$$K_{pm} = K_{pCO2}Y_{CO_2} + K_{pH2O}Y_{H_2O} \qquad , \qquad (27)$$

where

$$K_{pk} = K_1 + K_2T + K_3T^2 + K_4T^3 + K_5T^4 + K_6T^5 + K_7T^6 + K_8T^7 ,$$
$$(28)$$

subcript, k, stands for CO_2 or H_2O, and K_1 to K_8 are known constants.

3.5   Combustion Reaction

Combustion of an alkane fuel is assumed to take place in a single step to produce stochiometric amounts of carbon dioxide and water as the only products according to

$$C_sH_{2s+2} + (3s+1)/2O_2 = sCO_2 + (s+1)H_2O . \qquad (29)$$

Therefore, the production rates of CO_2 and H_2O and consumption rates of O_2 are proportional to the rate of combustion of fuel, W_k, which is given by Westbrook et al. (1982) as

$$W_k = k_cC_k , \qquad (30)$$

where k_c is a pseudo first-order kinetic constant.   It is given by

$$k_c = A\exp(-E_a/RT)C_{O2}^m C_f^{n-1} , \qquad (31)$$

where E_a is activation energy and ΔH_c is the heat of combustion per gmole of fuel consumed. The constants m and n are given by Westbrook et al. (1986) for several aliphatic hydrocarbon fuels. The energy release rate per unit volume, HRR_v, is given by

$$HRR_v = \Delta H_c W_k/Av . \qquad (32)$$

3.6   The boundary conditions

The above partial differential equations require specification of boundary conditions on all the dependent variables ρ, u, v, P, E, and C_k at inlet, outlet, upper and lower walls of the channel.

3.6.1.   At inlet, x=0 and all y values:

The inlet velocity components u_0 total energy E_0 density ρ_0 and composition as number densities, C_{k0} are specified. These boundary conditions assume that the inlet is far from the combustion zone so that they are affected by the changes occurring inside the computational domain. The inlet pressure P is unknown. The pressure is expected to change along the channel due to momentum boundary layer development along the channel walls due to friction. However, this pressure change is expected to be small compared to pressure change near the leading edge of the porous plate. Therefore, we specify that the inlet pressure drop to be zero. They are written as

$$u(t,0,y) = u_0, v(t,0,y) = 0, E(t,0,y) = E_0 , \qquad (33)$$

and

$$\rho(t,0,y) = \rho_0, C_k(t,0,y) = C_{k0}, \frac{dP}{dx}(t,0,y) = 0 . \qquad (34)$$

3.6.2   At outlet, x=L and all values of y:

Again we assume that the channel outlet is far from the combustion zone so that the outlet conditions are not affected by the changes taking place inside the channel. We set all the gradients to zero. The outlet pressure gradient, however, must be specified to obtain unique solution to the equations. We assume the outlet pressure to be atmospheric. In reality, however, combustion heat is released all the way to the end of the channel, affecting the outlet conditions. But the heat released is less than one tenth of the maximum heat release rate. These approximations are expected to be accurate for high fluid velocities, which exist in forced convection boundary layers. As the inlet velocity decreases, they become less accurate and the solutions near the end of the channel (1-2 cm near exit) are not accurate. The boundary conditions are written as

$$\frac{du}{dx} = \frac{dv}{dx} = \frac{dE}{dx} = \frac{d\rho}{dx} = \frac{dC_k}{dx}(t,L,y) = 0 , \qquad (35)$$

and

$$P(t,L,y) = P_{atm} , \qquad (36)$$

13

where $L=L_1+L_2+L_3$.

3.6.3 On top solid wall and non-porous sections 1 and 3 of the bottom wall y=H, y=0:

The top wall is assumed to be far enough from the combustion zone so that no heat is transferred to it from the flame. However, there is no slip on the wall and no mass flow through it. They are written as

$$\frac{dE}{dy} = \frac{d\rho}{dy} = \frac{dC_k}{dy} = \frac{dP}{dy}(t,x,H) = 0 , \qquad (37)$$

and

$$u = v(t,x,H) = 0 , \qquad (38)$$

for all values of x.

3.6.4 At impermeable sections of the bottom wall, y=0

The bottom wall is assumed to conduct heat away from the flame following Newton's law of cooling with a characteristic heat transfer coefficient h_w. As a result of this boundary condition, the wall will heat up to a temperature T_w, which varies along the wall and is calculated by an iterative method. The adiabatic and constant wall temperature boundary conditions, which were used in the existing works by Mao et al. (1984), Kodama et al. (1987), Chen and Tien (1986), and Ha et al. (1991) occur as special cases for $h_w=0$ and ∞ respectively. The boundary conditions are written as

$$h_w\left(T(x,0) - T_{atm}\right) = \lambda \frac{dT}{dy}(t,x,0) , \qquad (39)$$

$$\frac{d\rho}{dy} = \frac{dC_k}{dy} = \frac{dP}{dy}(t,x,0) = 0 , \qquad (40)$$

and

$$u = v(t,x,0) = 0 , \qquad (41)$$

for $x < L_1$ or $x > L_1+L_2$.

3.6.5 On the porous section of the bottom plate, y=0:

A mass balance for the fuel across the plate states that the injection rate of fuel input to the bottom side of the wall, as measured by the rotameter in experiments, should equal the total flux of fuel leaving the top side of the wall as shown in Figure 2. The total flux consists of diffusive flux and convective flux. We also assume that the plate is permeable only to fuel and no other species are transported across it. These boundary conditions uniquely determine the specie concentrations at the wall, which are unknowns and vary along the wall for uniform fuel injection rate, $\dot{m}$. An iterative method is used to calculate the specie concentrations on the surface. Kodama et al. (1987) assumed a constant and uniform concentration of fuel and other species at the wall rather than determining them as unknowns for PMMA. The boundary conditions are written as

$$\dot{m} = \frac{D\rho}{(1 - X_k)} \frac{dX_k}{dy} , \qquad (42)$$

for k=3,

$$X_k = \frac{D\rho}{\dot{m}} \frac{dX_k}{dy} , \qquad (43)$$

for k=1,2,4,5,

$$h_w \left(T(x,0) - T_{atm} \right) = \lambda \frac{dT}{dy}(t,x,0) , \qquad (44)$$

$$\rho(t,x,0) = \frac{P(t,x,0)}{RT(t,x,0)} , \qquad (45)$$

$$V_w = \frac{\dot{m}}{\rho(t,x,0)}, u(t,x,0) = 0 , \qquad (46)$$

and

$$E(t,x,0) = \rho(t,x,0)C_p(t,x,0)T(t,x,0) , \qquad (47)$$

for $L_1 < x < L_1 + L_2$.

heat feed back from the flame
$$\lambda \frac{\partial T}{\partial y}$$

heat loss $h_w(T_w - T_\infty)$

diffusive flux+convective flux
$$D\rho \frac{\partial X_w}{\partial y} + \dot{m}(1 - X_w)$$

fuel injection rate $\dot{m}$

interface@T_w, X_w
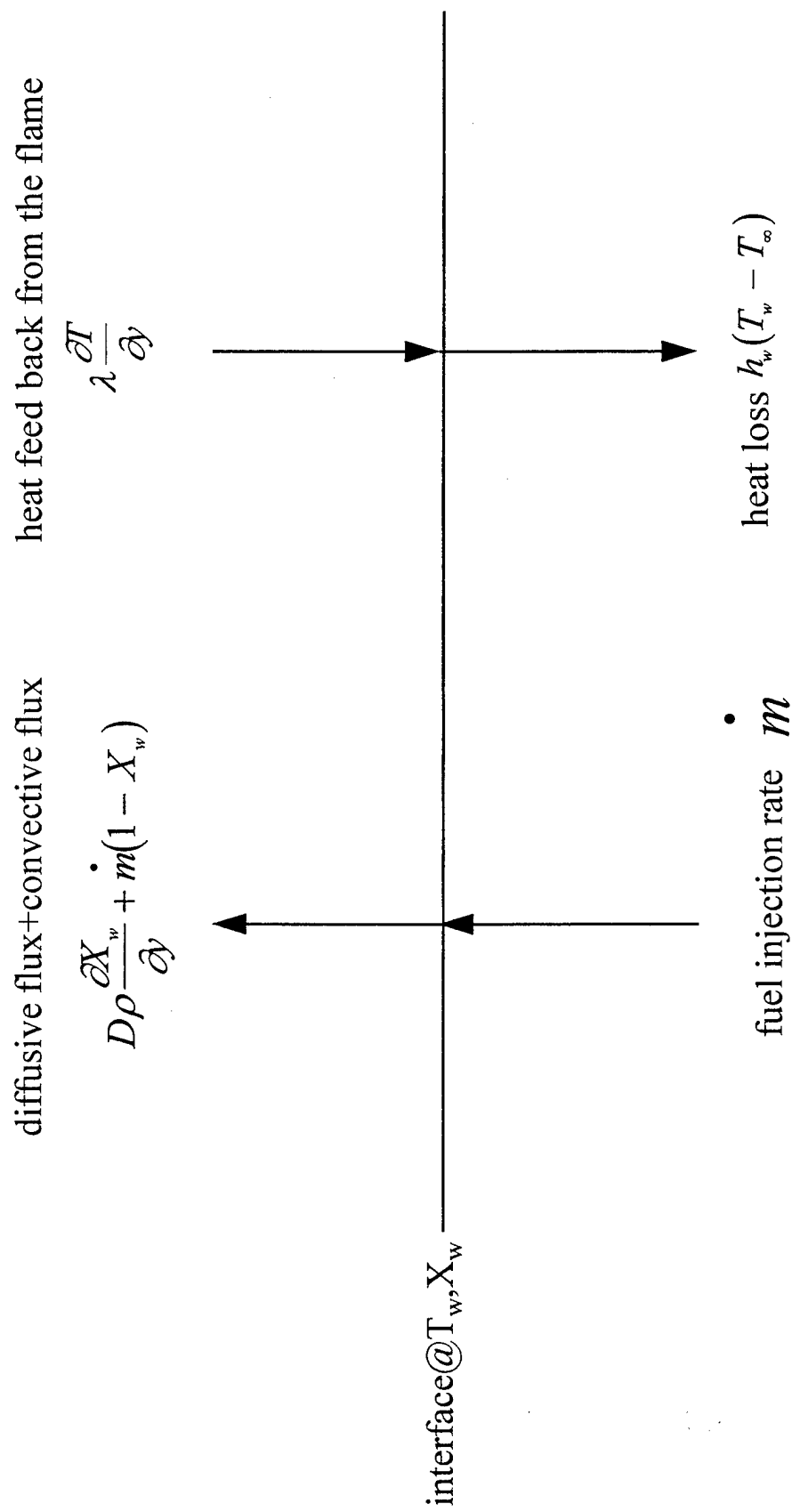
Figure 2   Schematic of the interfacial flux balance

3.7   Initial conditions

Initial conditions are taken as the inlet conditions at x=0 over the entire domain. Therefore,

$$u(0,x,y) = u_0, v(0,x,y) = 0, E(0,x,y) = E_0 , \qquad (48)$$

and

$$\rho(0,x,y) = \rho_0, C_k(0,x,y) = C_{k0}, P(0,x,y) = P_{atm} . \qquad (49)$$

4.0   NUMERICAL SOLUTION

There are several unknowns, i.e., ρ, u, v, P, E, Ck in the gas phase, as well as temperature and specie concentrations at the permeable plate. All of these must be calculated as functions of position x and y and time t. One typically specifies inlet velocity u_0, density ρ_0, composition C_{k0}, and temperature T_0 (or energy E_0) of the air. Also, one specifies the mass injection rate $\dot{m}$, composition C_{kw}, density ρ_w, of the fuel, and the wall heat transfer coefficient h_w. The temperature T, is calculated from the pressure P, using the ideal gas law given by equation (16).

The equations are discretized by a finite volume method on a grid shown in Figure 3. Figure 3 shows the Eularian domain containing about 200x150 finite volume cells in x and y directions respectively. The cells are clustered closely near the leading edge of the porous section. Typical cell size inside the flame is 0.2 cm x 0.4 cm. The cells are stretched in both directions from the leading edge. The equations are discretized by finite volume approximation. The convective, diffusive, combustion, and radiation contributions are solved by separate algorithms using separate time steps, which are typically either smaller or equal to the global time step. Diffusion and reaction processes are subcycled within a global time step and cumulative contributions from each process are calculated. These terms are then coupled together by time-step splitting as discussed by Oran and Boris (1987). The global time step is chosen such that the diffusion processes are not subcycled by more than three times and is typically of the order of 10 msec during ignition and 50 msec after ignition.

Convection equations are solved by the high-order implicit algorithm, Barely Implicit Correction to Flux-Corrected Transport (BIC-FCT), which was developed by G.Patnaik et al.(1986) to solve the convection part of the equations for slow flows. The Flux-Corrected Transport (FCT) is an explicit scheme for the solution of hyperbolic equations. Therefore, it requires very small time steps dictated by sound speed following Courant-Friedrichs-Lewy
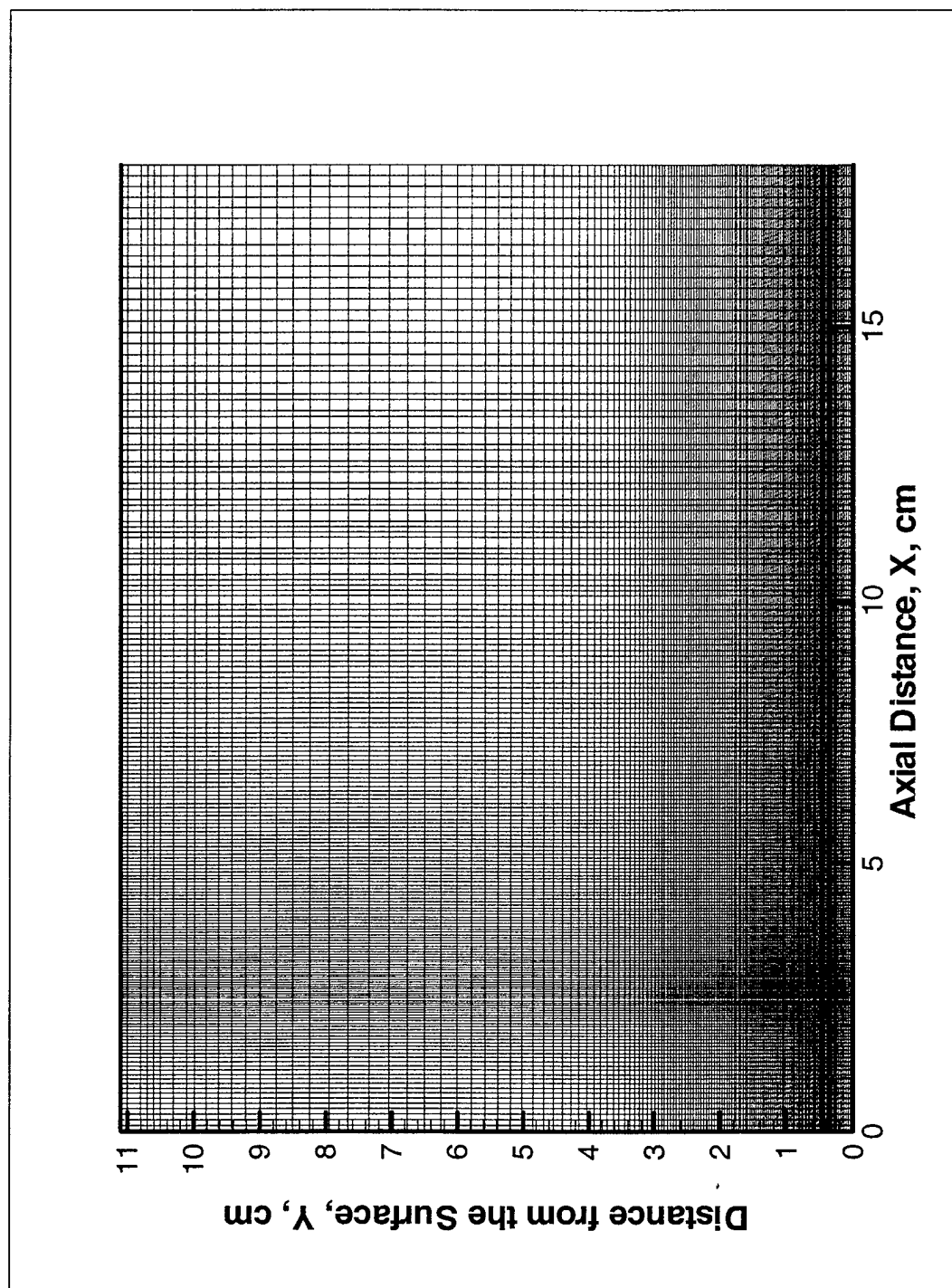
Figure 3   Numerical mesh with smallest cells concentrated near the leading edge of the porous plate and cells stretched in both directions x and y

condition. BIC-FCT was developed based on the suggestion by Casuli and Greenspan (1984) that only the pressure in momentum equation and velocity in energy equations need to be treated explicitly to increase the time step to that based on fluid velocity rather than the sound speed. This method involves solution of an elliptic equation for pressure which is solved using MGRID algorithm discussed in detail by DeVore et al.(1984). Typically, the global time step is much smaller than the convection time step and the courant number based on maximum fluid velocity and minimum cell size is much smaller than 0.3.

Parabolic diffusion equations are discretized using explicit finite difference approximations. The time steps for the subcycle are calculated based on minimum cell size and maximum diffusivity in the domain. If these time steps are more than one third of the global time step, then the global time step is reduced. At the end of each subcycle, diffusion contributions to specie concentrations, temperature, and momentum are updated for mass, heat, and momentum diffusion, respectively. Power law models are fitted to the Lennard-Jones potentials a priori and are then used to calculate the viscosity, conductivity and diffusivity of each specie in a given cell as functions of local gas temperature.

Reaction contribution is described by a single nonlinear stiff ordinary differential equation and is solved by using Burlich-Stoer algorithm with Rhomberg interpolation as described by Press et.al. (1986). Unlike the diffusion processes, the reaction time steps are evaluated based on local values of the variables rather than global maximum/minimum values in the domain. The time steps are calculated cell by cell from the local values of rate constant and specie concentrations and temperature and vary widely across the domain. Typically, the time steps can be hundreds of times smaller than the global time step, especially during ignition near the leading edge of the porous plate. After ignition, the time step increases by a factor of 3-10 in the hottest regions. Therefore, the reaction calculations are subcycled to a varying degree within the domain. Specie concentrations are updated at the end of each subcycle. A very significant cost of computation is incurred in reaction calculations.

4.1   Fixed Point Iterative Scheme

The boundary conditions are generally implemented by introducing ghost cells adjacent to the boundary. The details of the implementation were discussed elsewhere by Oran and Boris (1986). However, the boundary conditions at the solid surface, given by equations (42)-(44), require special attention since they are implicit and require an iterative procedure. A fixed point iterative scheme is used as described by Burden and Faires (1985). Conceptually, the diffusive and convective fluxes at the solid surface are calculated such that equations (42)-(44) are satisfied at the end of each time step. These fluxes are used as boundary conditions for obtaining solutions to the convection and diffusion equations for the next time step within the time step splitting scheme. This is achieved by rewriting equations (42)-(44) as

$$h_w\left(T_w^{n+1}(t,i) - T_{amb}\right) = \lambda^n(t,i,1)\left(T^n(t,i,1) - T_w^{n+1}(t,i)\right)/\Delta y, \qquad (50)$$

for fuel, k=1,

$$\dot{m}\left(1 - X_{wk}^{n+1}(t,i)\right) = D^{n}(t,i,1)\rho^{n}(t,i,1)\left(X_{wk}^{n+1}(t,i) - X_{k}^{n}(t,i,1)\right), \qquad (51)$$

for species other than the fuel, $k \neq 1$, and

$$\dot{m}\left(X_{wk}^{n+1}(t,i)\right) = D^{n}(t,i,1)\rho^{n}(t,i,1)\left(X_{wk}^{n+1}(t,i) - X_{k}^{n}(t,i,1)\right), \qquad (52)$$

where, quantities with superscripts n and (n+1) are the values at iteration n and n+1 , and quantities with subscript w are the values at the solid surface. Quantities with subscript i are the values at cell number i along the plate. The mass injection rate $\dot{m}$, heat transfer coefficient h_w, and time t, are fixed in equations (50)- (52). Note that the bulk values of temperature T(t,i,1), and composition X(t,i,1), are implicit functions of interface values T_w (t,i) and X_{wk}(t,i).

At the end of iteration n, all of the values in equations (50)-(52), except T_w^{n+1} and X_{wk}^{n+1} are known. Therefore, equations (50)-(52) can be used to calculate T_w^{n+1} and X_{wk}^{n+1} for the next iteration (n+1). These interfacial values for temperature and gas composition are first compared with the values used in the previous iteration n. If the difference is more than the error limit (0.1 %), the new interfacial values for temperature and composition are used to calculate the boundary values of the diffusive and convective fluxes. These boundary fluxes are then used for reintegrating the differential equations with all of the dependent variable set to the values at the beginning of the time step. This gives values of temperature T^{n+1}(t,i,1), and composition X_k^{n+1}(t,i,1) at the next iteration (n+1). This iterative procedure is continued until convergence is obtained and the calculations are moved to the next time step. Typically, it takes about seven iterations/timestep during ignition and 3 iterations/timestep after ignition for iterations to converge at the end of a time step. In this procedure, the interface is treated as a discontinuity without any thickness, a well accepted approximation in the interfacial transport literature. All of the conditions at the interface are satisfied at every time step unlike "interfacial condition" imposed by earlier works. Previous works consider interface with finite volume, therefore allowing accumulation as well as transverse (x-direction) transport through that volume. Therefore, the interfacial conditions are expected to be strictly valid only at steady state where all accumulation terms vanish. Furthermore, the heat-loss boundary condition given by equation (42) is significantly different from the previous works, which used constant surface temperature. It is more realistic and affects the flame to surface heat feedback especially near the leading edge.

The interfacial values of temperature and specie mass fraction are obtained as part of the solution along with the values of all of the dependent variables as functions of position and time. Next, we will describe the solution for given values of   , U_0, h_w, L_1, L_2, and L_3. U_0 and   are kept uniform along the inlets of the channel and porous section respectively.

20

5.   DISCUSSION

First, we will discuss transient solutions briefly, followed by a discussion of the steady state results. We will present a full and detailed discussion of the steady state solutions for temperature, heat release rates, density, pressure, fluid velocity, and specie concentration distributions. We will also discuss specie concentration profiles along the surface and heat feed back from the flame to the burner surface.

5.1   Transient Flame Development

The numerical solutions are time-dependent and can describe the entire development of the flame from ignition to steady state, once an initial condition is prescribed. In these simulations shown in Figure 4(a-h), the porous section is located between x=5 cm and x=10 cm (L_1=5 cm, L_2=5 cm). The leading section x<5 cm is adiabatic (h_w=0), the porous section (5<x<10) is kept at a uniform temperature of 700 K, and the rest of the plate (x>10 cm) is kept at room temperature (h_w=∞). Initially (t=0-), only air flows past the plate at a velocity of u_0=30.0 cm/sec and no fuel is present in the system. At time, t=0+, ethane gas is injected through the porous plate uniformly at a fixed mass flow rate of $\dot{m}$ = 3.44e-03 gm/cm^{2}sec. At the same time external heat is added to several cells above the leading edge of the porous plate for 2000 time steps for a total of 20 msec. At the end of 20 msec the external heat addition is stopped and spontaneous combustion of the fuel gas begins to occur.

From time t=0, fuel is ejected from all across the porous surface at a fixed mass rate and diffuses into the flowing air stream creating a partial mixture of fuel and air just above the entire length of the plate. The external heat raises the local gas temperature and increases the local reaction rate, which are related exponentially by Arrhenius law, in a few cells above the leading edge of the porous plate. Thus, the partially mixed fuel and air in those cells are converted to carbon dioxide and water releasing heat at a rate, HRR_v. This heat further raises the local gas temperature establishing a self-feeding loop. Figure 4a shows the temperature and rate of heat released due to the combustion reaction at the end of the ignition step. The y- axis represents distance from the surface of the plate. The temperature is indicated by the color contours with red being the hottest and white being the coldest. Also shown in Figure 4a is a single contour (1e+06 ergs/cm^3 sec) of heat release rate HRR_v. This represents the region in which most of the combustion taking place converting oxygen and fuel to carbon dioxide and water. The temperature gets to about 1200K at the end of the ignition step.

The local gas temperature continues to rise due to continued generation of heat by the combustion reaction. The region contained in the HRR_v contour is relatively hot as indicated by the red color, while the plate and bulk of the gas are relatively cold as shown in Figure 4b. Therefore, the heat is conducted away from the flame region to the surrounding gas and is also convected by the bulk flow in the x-direction to downstream of the plate. This raises the temperature downstream by propagating combustion. Thus, the flame propagates across the plate as shown in Figure 4b. Figure 4b shows that the flame is anchored near the leading edge of the porous plate while the right arm of the flame propagates into the gas downstream. The leading plate (L_1) is adiabatic. Therefore it can reach relatively high temperature, while the porous plate
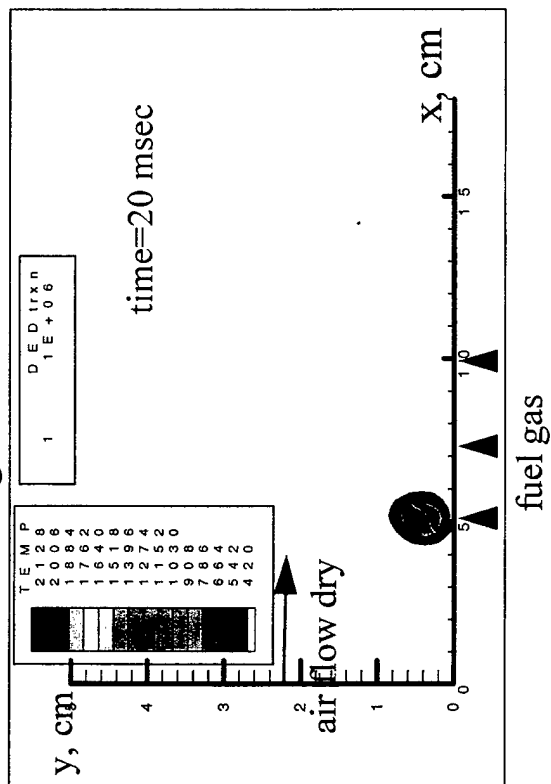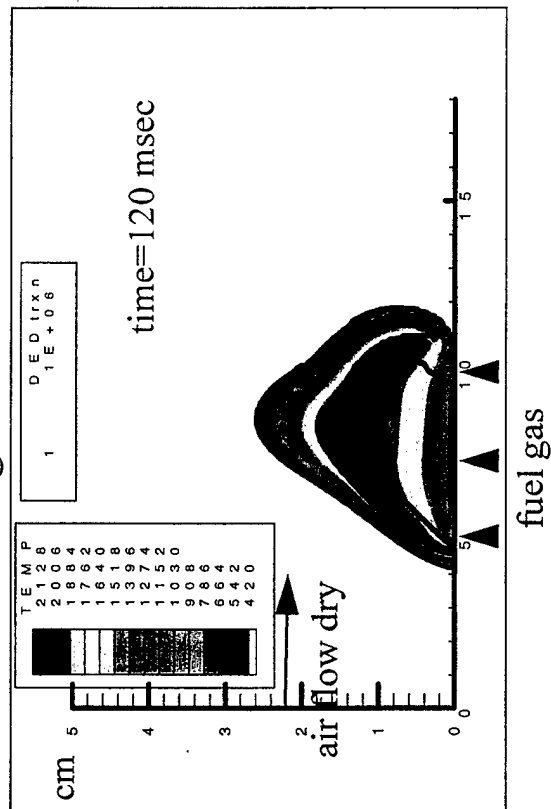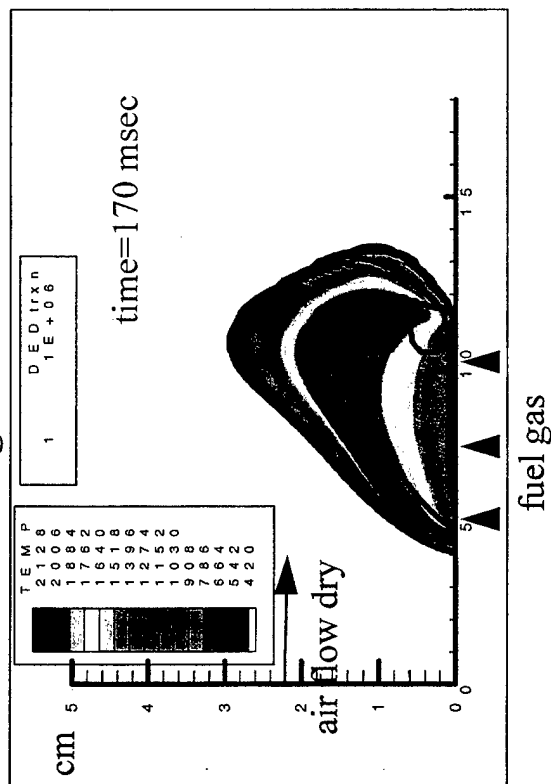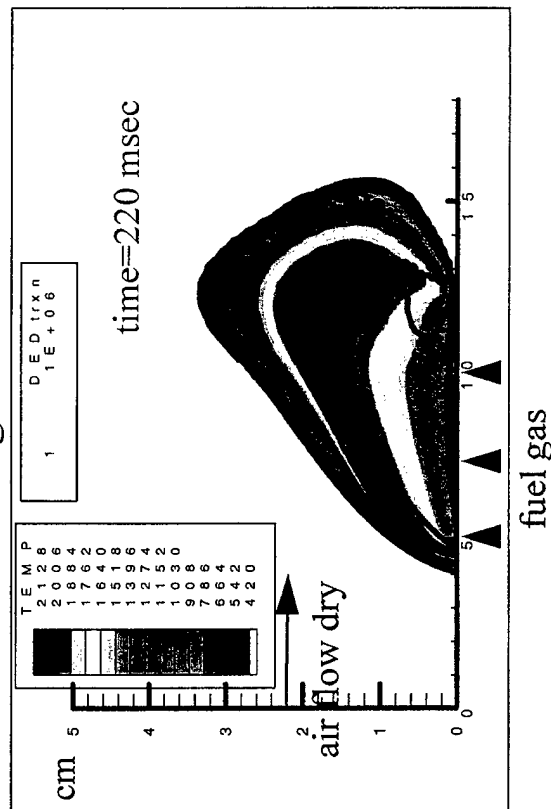
Figure 4a

Figure 4b

Figure 4c

Figure 4d

Figure4a-d Evolution of Thermal (K) and Heat Release Rate (ergs/cm³sec) Profiles After Ignition Near the Leading Edge of the Porous Plate (with adiabatic leading plate)
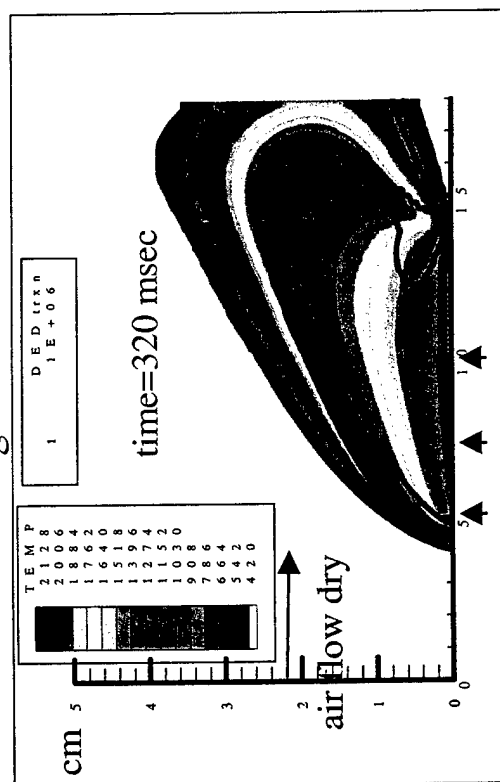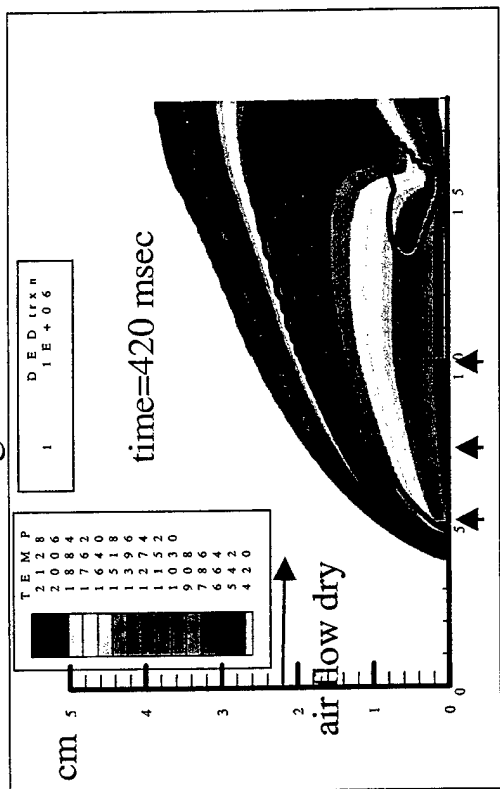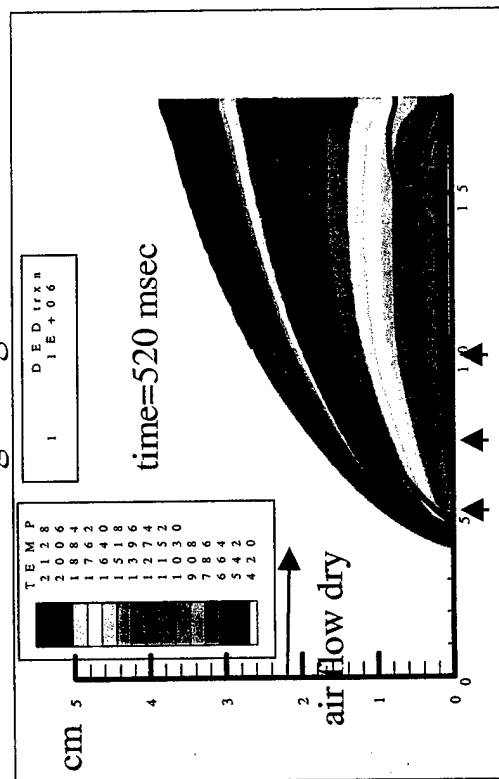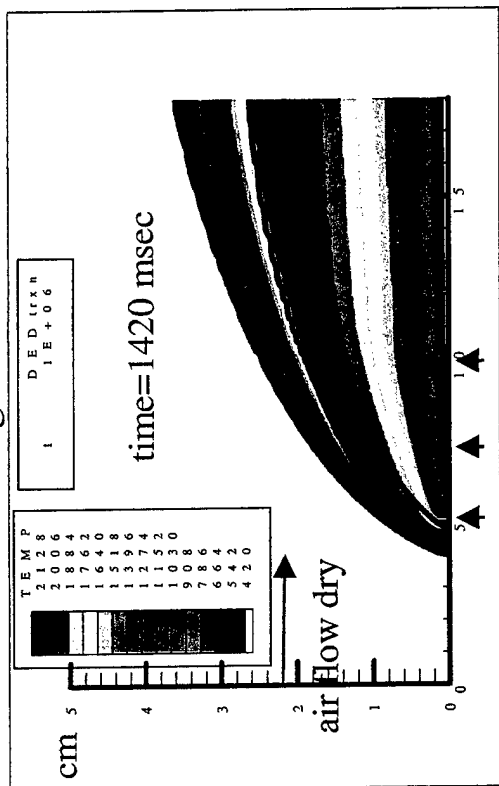
Figure 4e

Figure 4f

Figure 4g

Figure 4h

Figure 4e-h   Evolution of Thermal (T, K) Contours, After Ignition Near the Leading Edge of the Porous Plate (with adiabatic leading plate), With Time, t. Also Shown is a Single Heat Release Rate (HRR$_v$, ergs/cm^{3}sec) Contour

loses heat to the ambient through the back of the plate. The HRR_v contour in Figure 4b also shows a triple flame structure at the downstream end of the flame. This is because the flame propagates into an already mixed gas of fuel and air. Fuel is injected uniformly across the entire plate and the fuel from the plate already had 120 msec to diffuse into air forming a partial mixture in front of the propagating arm of the flame. Figure 4b shows a main stem, a long right arm and a very short left arm. Figure 4b contains fuel on both sides of the main arm of the triple flame structure. This may be due to expansion flow that pushes against the incoming fuel flow and the plate dispersing the fuel to both sides of the triple flame. The region between the Figure mainstream and the short left arm is fuel rich while the region between the main stem and right arm is fuel lean. Thus the reaction zone develops a complex structure near the solid surface, which is relatively cold due to heat loss, while the flame is very well anchored to the surface near the leading edge, which is adiabatic and no heat is allowed to pass through. Both the HRR_v and temperature contours show spread of flame covering the entire porous plate.

Figure 4c shows propagation of the flame beyond the porous plate as the fuel and air are convected downstream. The HRR_v contours in Figure 4d and 4e show that the flame moves relatively slowly near the surface of the plate due to no-slip at the wall, while farther from the plate the HRR_v contour reaches farther downstream. They also show weakening of the right arm of the triple flame as the products are produced and convected downstream. The HRR_v contours in Figure 4f show continued weakening of the right arm of the triple flame and the flame begins to transform from a closed flame to an open flame. Finally, at time=1420 sec, Figures 4g-h show that the flame completely opens as the steady state is reached. One notices that the flame extends far beyond the porous plate with temperatures being relatively high. The temperatures in the reaction zone near the leading edge no longer continue to increase. Instead they reach a maximum of about 2100 K. This is because the density is reduced as the temperature increases following the ideal gas law. Also, the absolute concentrations of all of the species are reduced. Furthermore, products dilute the gaseous mixture and reduce the reactant concentration further. Thus, the reduced concentrations of the reactants tend to decrease the reaction rate and HRR_v, while the increased temperature tend to increase the reaction and HRR_v. When these two opposing mechanisms balance, the temperature and heat release rate reach a local maximum and do not undergo further change with time.

The flame spread rate is about 1 mm/sec along the porous section (L_2). It drops to about 0.2 mm/sec along the non-porous section (L_3) due to the absence of fuel injection and lower surface temperature. As one might expect, the spread rate along the porous section is much higher than that observed (~1 mm/min) on a PMMA surface in co-currant flame spread experiments. Next, we describe the steady state solutions, which are the main emphasis of this report in detail.

5.2   Steady State Solutions

The steady state solutions described below are obtained for n-pentane gas combustion. The porous section is located between x=2.45 cm and x=9.5 cm (L_1=2.45 cm and L_2=7.05 cm). The fuel injection rate is   =3.44e-03 gm/cm^2sec, the lower plate heat transfer coefficient is h_w=6.92e04 $ergs/cm^2sec$, and the inlet air velocity is u_0=60.0 cm/sec.

5.2.1   Heat Release Rate and Temperature Profiles

Figure 5 shows the energy release rate contours. The heat is released inside a thin band above the plate where a mixture of fuel and oxygen exist due to diffusion and convection of fuel ejecting from the surface and air flowing across the surface. The combustion of this fuel-air mixture releases energy at a rate that depends on the product fuel and oxygen concentrations as shown by the rate expression given by equations (30) and (31). In the region above the thin band displayed in Figure 5, fresh air exists containing no fuel and below this region is fresh fuel containing no oxygen. Therefore, reaction occurs only within the thin region releasing heat at a rate that varies over three orders of magnitude along the plate. The HRR_v drops more steeply on the air side of the rate contours than on the fuel side, which is indicated by the blue band closer to the fuel side. This is because of higher temperature gradient on the air side than on the fuel side, and the HRR_v depends exponentially on temperature as shown by equations (30)-(31). Figure 6 shows the temperature contours in color, along with a single heat release rate contour as a black solid line. As the combustion energy is released, gases heat up and the temperature increases within the region contained by the HRR_v. The rise in temperature further increases the reaction rate. On the other hand, the concentrations of fuel and oxygen decrease due to consumption by the reaction, dilution by the products, and reduced density due to high temperature. The decreased concentrations of reactants tend to decrease the reaction rate. This results in the appearance of maxima in HRR_v and temperature profiles. The heat released is also conducted away from the flame into the bulk of the fuel below and bulk of air above. Therefore, the temperature profiles are wider than the heat release rate profiles.

Figure 7 shows the HRR_v and temperature profiles along the length of the plate at different distances from the surface y. They show that the heat released is the highest where temperatures are the highest as one might expect from the rate expression. The flame-to-surface distance is generally referred to as the flame standoff distance, δ_f. The flame standoff distance is the distance between the flame, as defined by the position of maximum in temperature with vertical distance from the surface. Clearly, this distance increases with x from 0.02 cm at x=2.5 cm to 1.0 cm at x=10.2 cm. The width of the HRR_v curve shows the thickness of the flame or the reaction zone, which increases by about a factor of 5 as x increases from 3 cm to 10 cm. Figure 8 shows the HRR_v and temperature profiles in the vertical direction. The temperature gradient at the surface (y=0) is proportional to the heat feedback from the flame to the surface. The heat feedback is a crucial quantity since it drives the pyrolysis process in combustion of solids. The gradient decreases with distance along the plate, x, due to the increased flame stand off distance. As the gradient reduces, the surface temperature also reduces as required by the surface boundary condition given by equation (39). Figure 8 also shows that, near the leading edge (x=2.45 cm), the maximum heat release rate and temperature increase along the flame in the heat up region (2<x<3.0) and then decrease. As x increases from 3 cm to 14 cm, the maximum flame temperature decreases by about 200 K due to heat loss from the flame region to the bulk. This temperature change leads to a decrease in maximum heat release rate by a factor of 10 due to the exponential relationship between them.
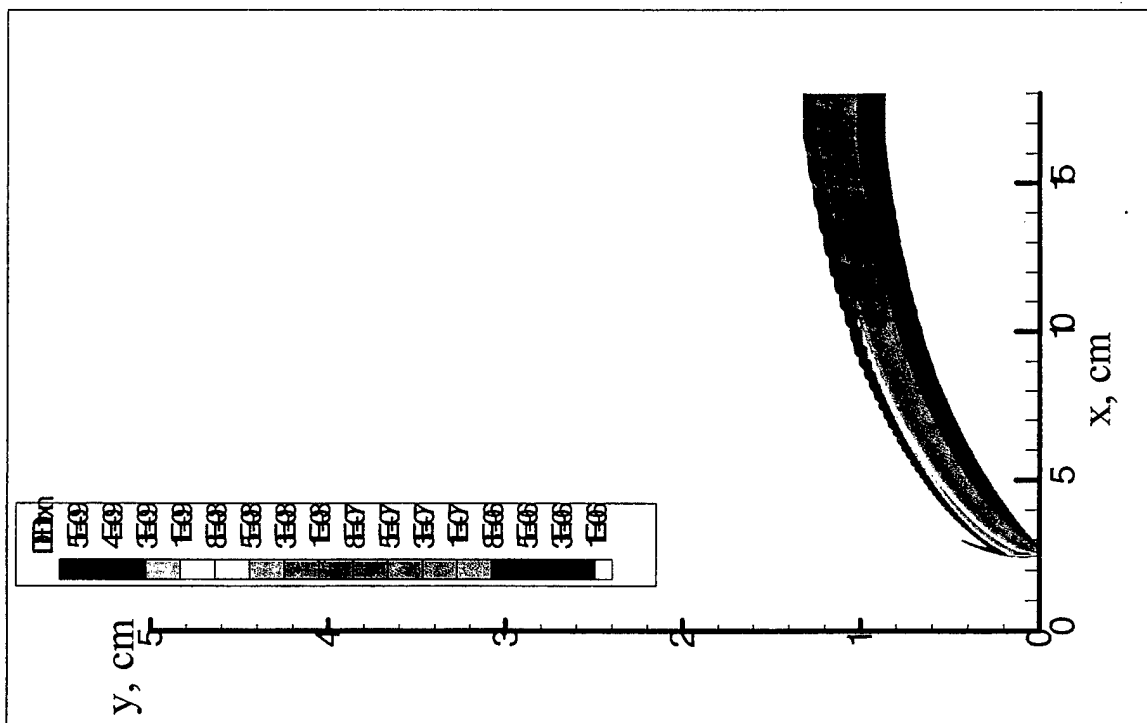
Figure 6   Temperature, K, Profiles
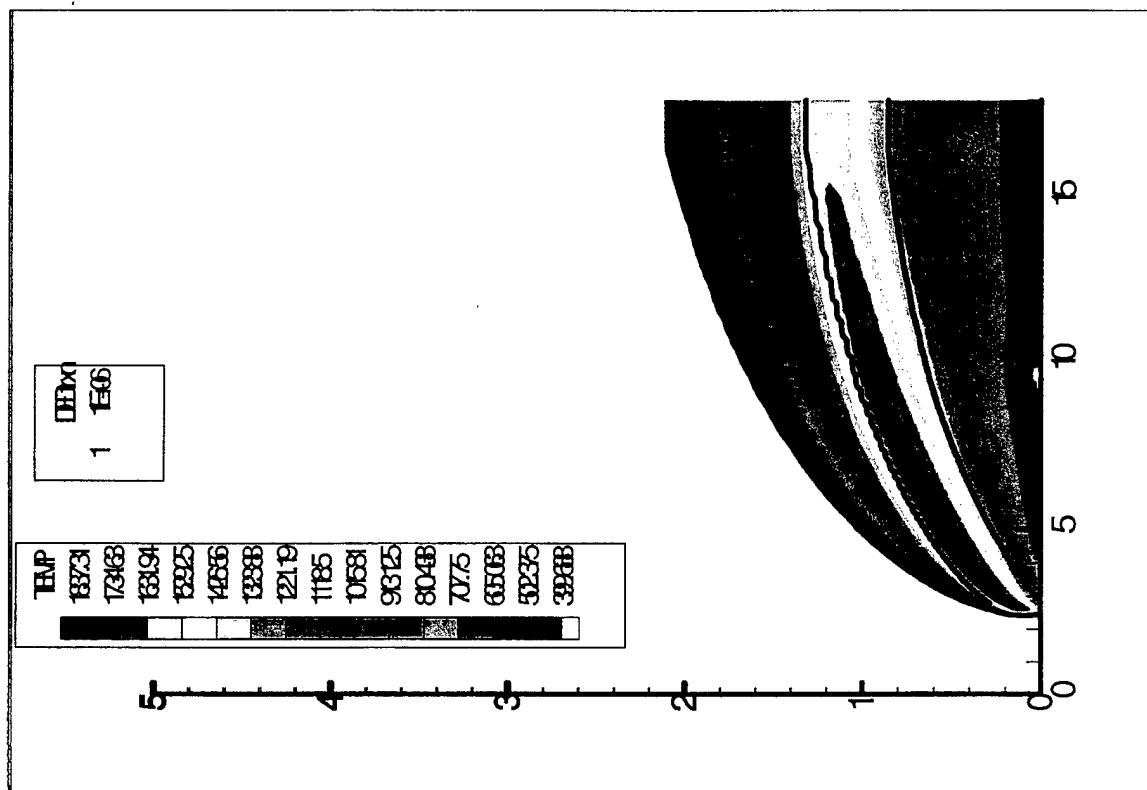

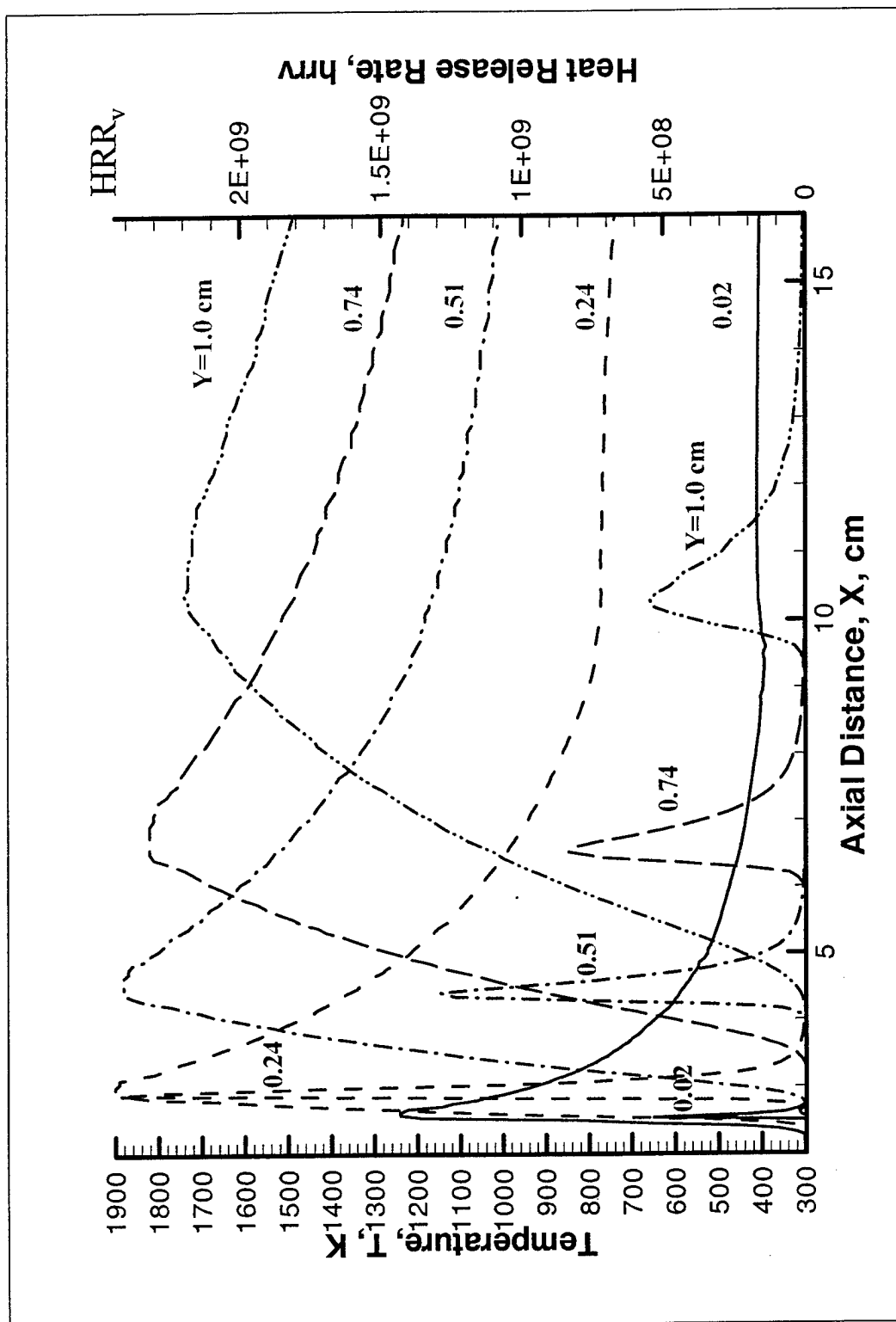Figure 5   Heat Release Rate (HRR$_v$) Profiles,
            ergs/cm^{3}sec

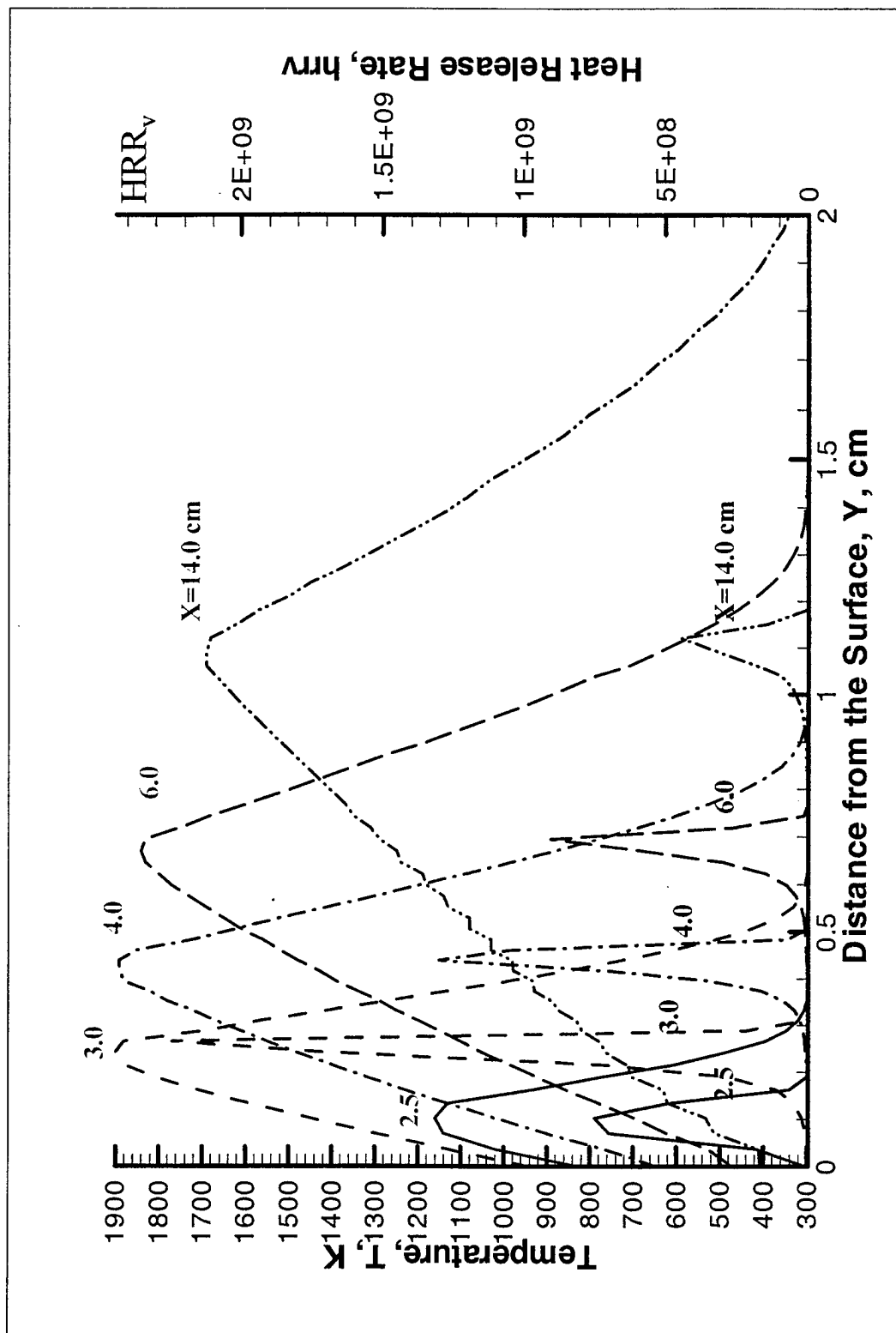Figure 7 Heat release rate (HRR_v, ergs/cm3sec) are in red, and temperature (K) are in blue with axial distance x

Figure 8   Heat release rate (HRR$_v$, ergs/cm3sec) are in red, and temperature (K) are in blue with vertical distance y

5.2.2 Density, Pressure and Velocity Profiles

As the temperature of the gases increase due to combustion, the density decreases according to the ideal gas law given by equation (16). Figure 9 shows low density in the flame region due to high temperature and high densities in the bulk of the fuel and air. It is to be noted that the density of the fuel is higher than air at a given temperature due to differences in the molecular weight. Therefore, the density at the porous surface, shown in red, is higher than in the bulk of the air, shown in yellow. The flame is contained in the heat release rate contour shown in black line in Figure 9. Figure 10 displays the pressure contours. The pressure is high near the leading edge of the porous plate, where HRR_v is the highest, and decreases with distance from the leading edge both in x and y directions. Clearly, air must travel against the rising pressure as it approaches the leading edge region toward the combustion zone and one may expect deceleration. It also moves upward since pressure decreases with y near the leading edge. Past the combustion zone, with the high pressure zone behind, the air travels in the direction of decreasing pressure and tends to accelerate. However, drag at the surface tends to prevent the air from accelerating.

The velocity fields are the result of complex interaction among gas expansion, air flow past the surface, fuel flow ejected from the surface, and drag at the surface due to no-slip condition. As the heat is released due to combustion, the gases expand perpendicular to the heat release rate contour away from the heat source. As shown earlier, the HRR_v is the highest near the leading edge of the porous plate, where fresh fuel and air meet. Therefore, the expansion effects are dominant near the leading edge and decrease quickly with distance from the leading edge, since the HRR_v drops off quickly with the distance. The incoming air encounters expansion flow in the opposing direction and moves upward as it approaches the leading edge of the porous plate, as shown by the velocity vectors in Figure 11. The upward movement gets smaller with distance from the leading edge both in x and y directions. Such a vector plot showing the diversion in air flow to the upper part of the flame was also shown by Kodama et. al (1987) and Chen and Tien (1986) in their theoretical studies of PMMA combustion.

Figure 12 shows the expansion effects on the x-component of the gas velocity. Closer the surface, the x-component of the velocity is influenced by the interaction among drag on the surface, expansion flow and main air flow. Note that the HRR_v contour is almost perpendicular to the plate near the leading edge and the expansion flow generated is mostly in the negative x direction upstream of the contour and in the positive x direction downstream of the contour. Figure 13 shows that u_x decreases from its inlet value due to drag on the non-porous section leading up to the porous plate. As the air approaches the fuel near the leading edge of the porous plate, u_x decreases further due to strong opposing expansion flow upstream of the heat source. Then ux recovers rapidly as indicated by the sharp raise in the profile downstream of the leading edge, where the expansion flow is in the same direction (x direction) as the main air flow. The velocity u_x decreases slowly with distance downstream of the leading edge due to drag exerted by the surface. Away from the surface, both the effects of expansion flow and surface drag reduce. Note that the HRR_v becomes small and the contour becomes flat and relatively parallel to the plate. Therefore, the expansion flow is much smaller in magnitude and is mainly in the y direction
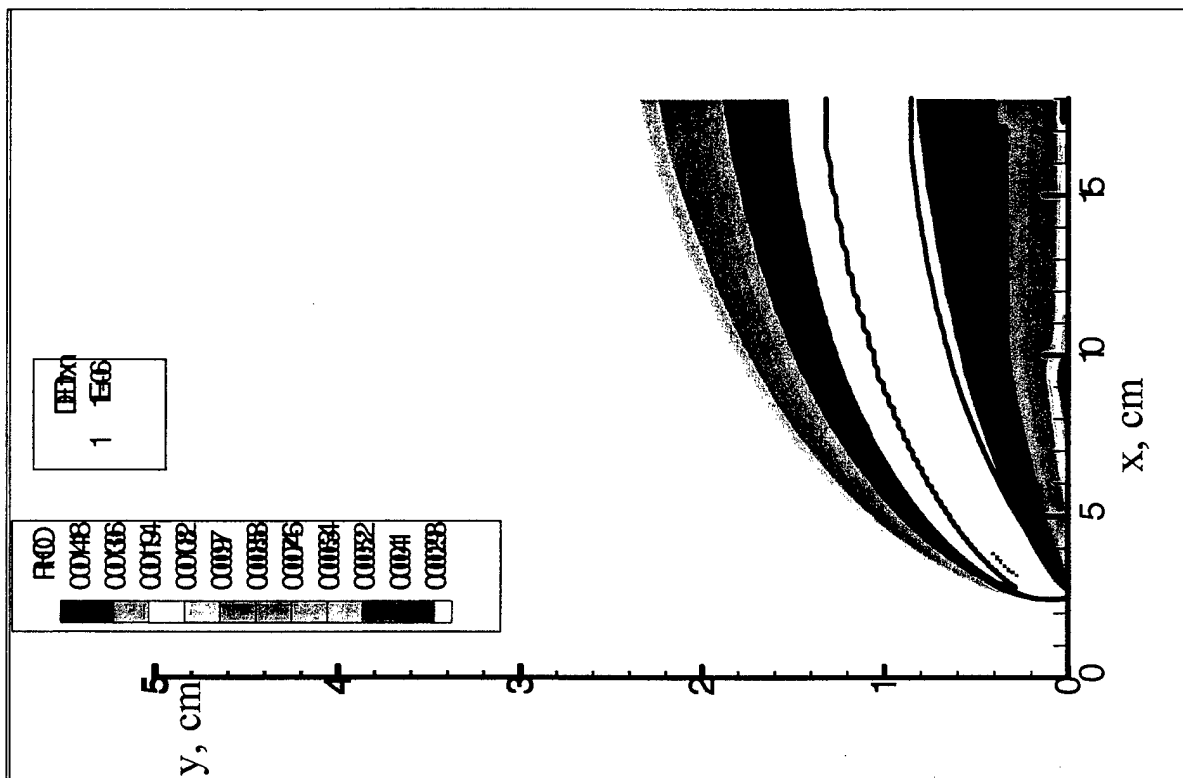
DP
3456
3233
2999
2766
2533
2299
2066
1833
1599
1366
1132
9095
6661
4327
2048

Figure 10 Pressure Contours, P-P$_{atm}$, Pascals

X

Y

RHO
0.0048
0.00036
0.00194
0.00082
0.0097
0.00038
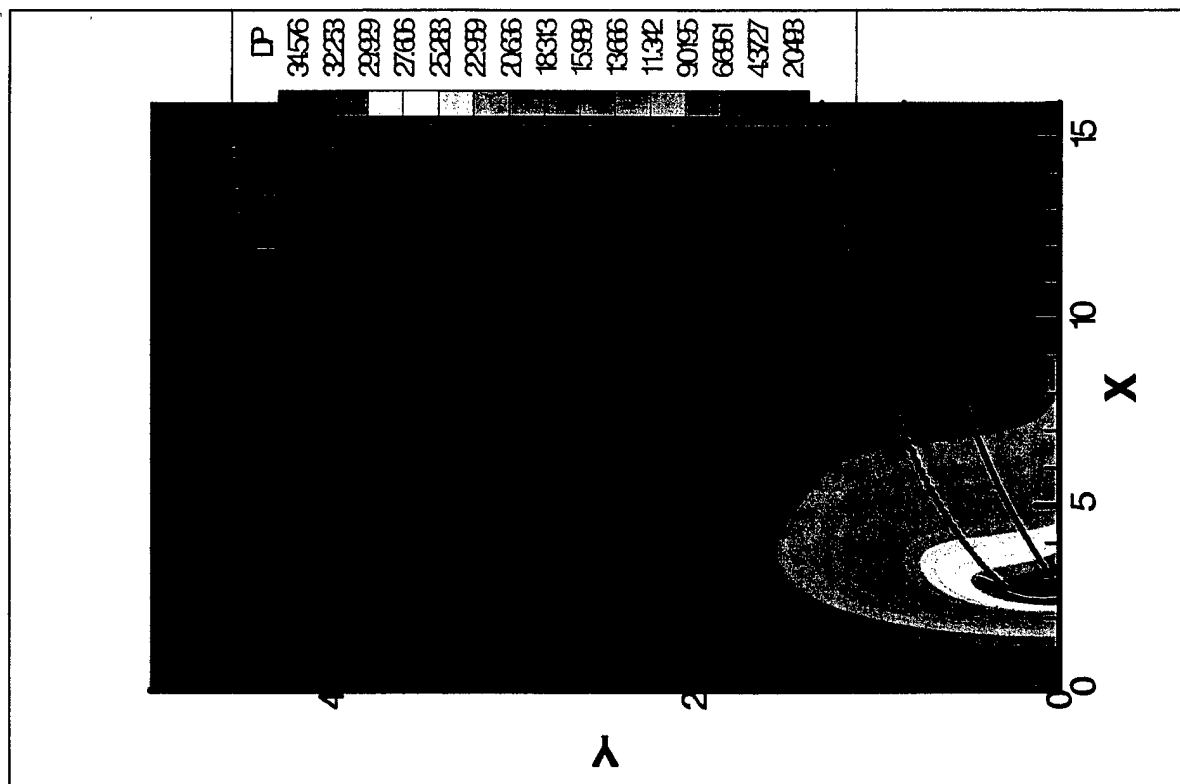0.00046
0.00034
0.00032
0.0004
0.00028

1E-06
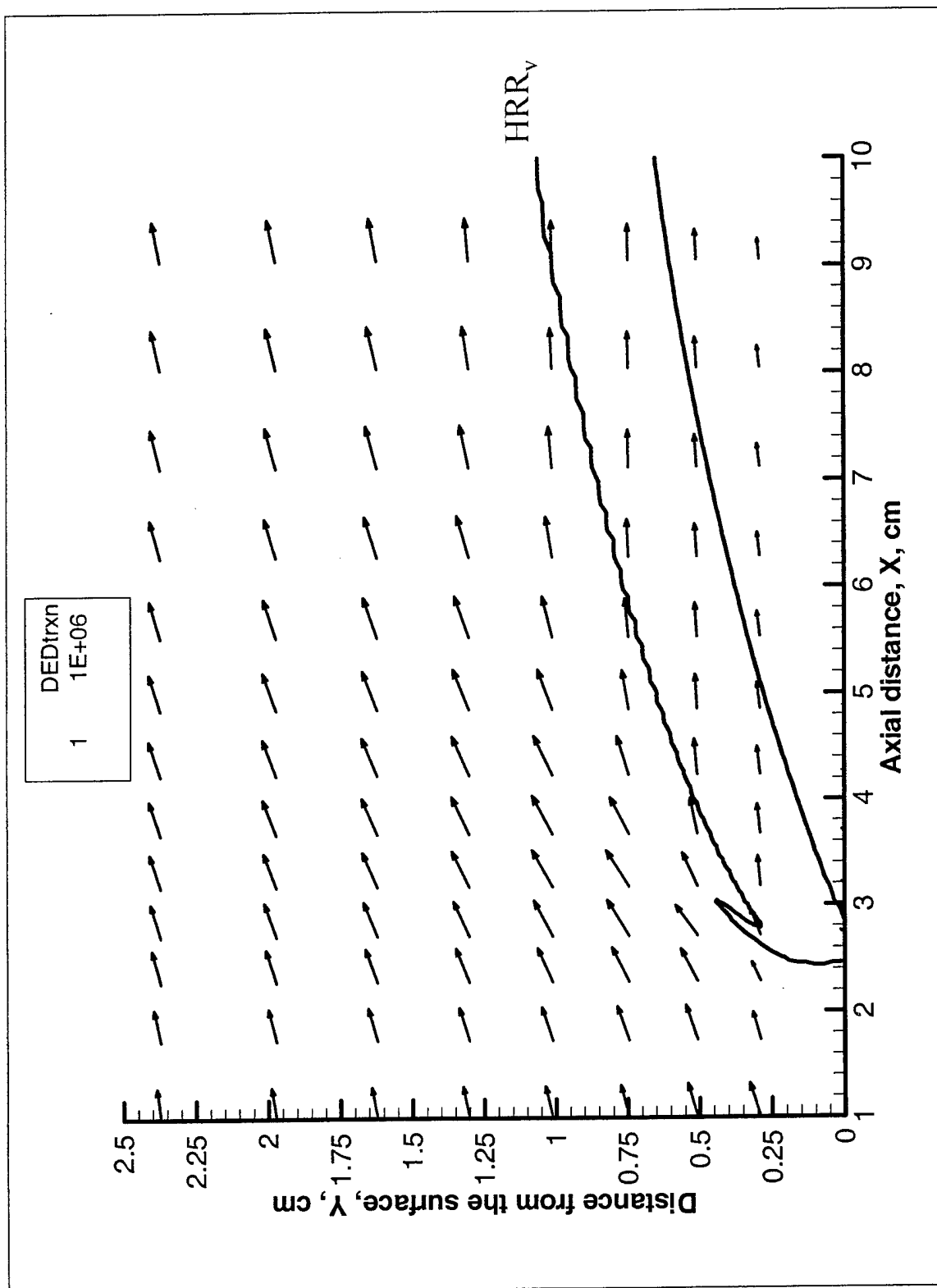
y, cm

x, cm

Figure 9 Density Contours, gm/cm^3

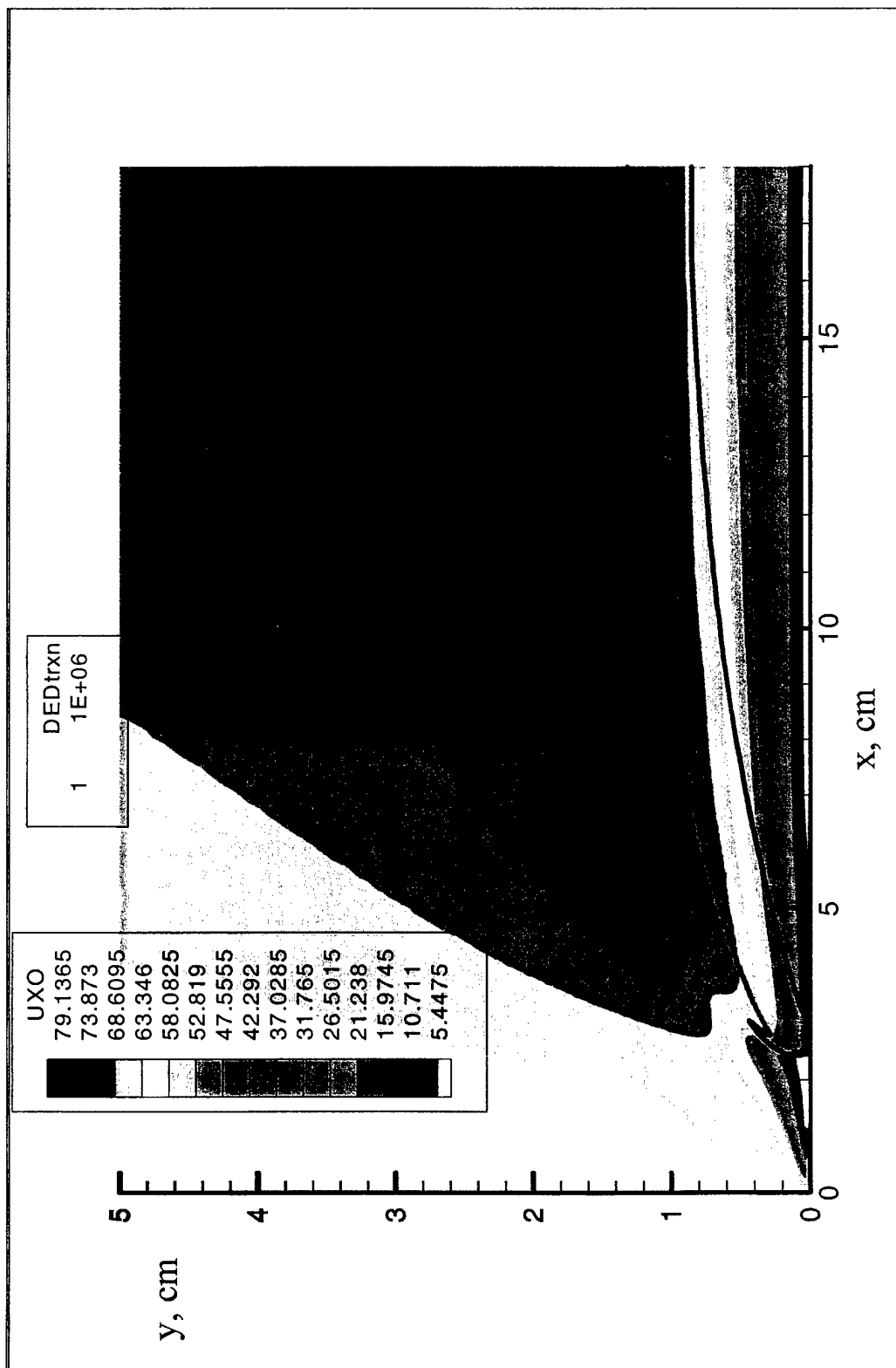Figure 11   Overlay of velocity vectors and heat release rate contour to show expansion flow induced by the reaction

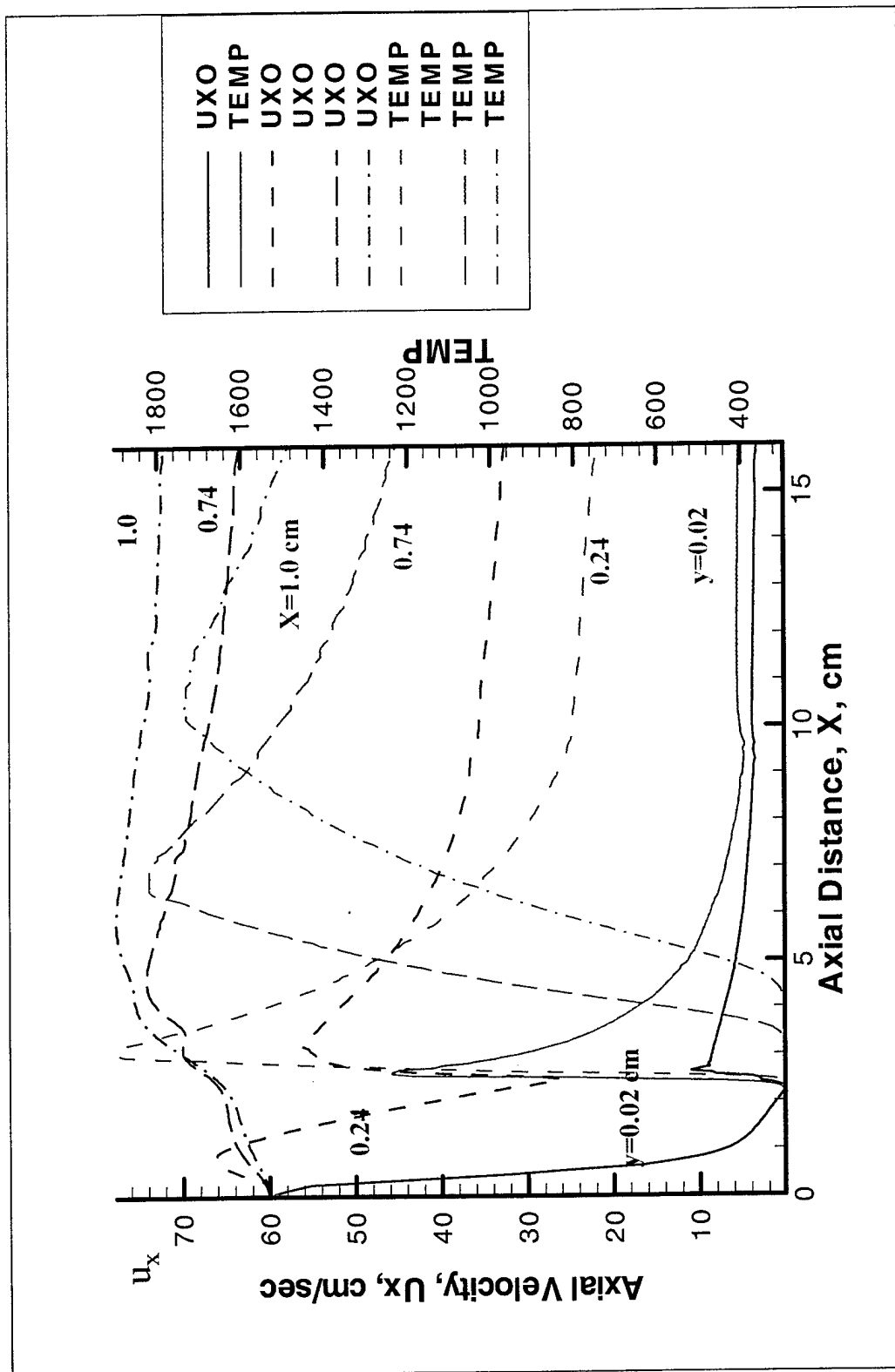Figure 12   Axial velocity (u_x, cm/sec) contours along with a contour of heat release rate

Figure 13 Axial velocity (u_x, cm/sec) are in red, and temperature (K) are in green with axial distance x

away from the contour. This leads to relatively flat u_x profile with distance along the plate. Indeed the velocity u_x increases slowly with x in the region outside of the thermal boundary layer and well above the combustion zone. This is due to the fact that total mass flowing through the channel must be a constant. Therefore, the velocity away from the surface must increase to compensate for the decrease in u_x near the surface. Figure 14 shows the u_x variation with distance perpendicular to the plate, y. The velocity u_x appears to increase above the inlet velocity of 60.0 cm/sec with y and then begins to come down at larger values of y. This has been referred to as the velocity "overshoot" in the literature by Ramachandra and Raghunandan (1986). The root cause for the velocity increase seems to be the gas expansion that diverts the flow upward near the leading edge rather than the effect of upper wall as proposed by Ramachandra and Raghunandan (1986). This gas expansion effect due to temperature rise can be seen clearly in Figure 15, which shows mass flow in the x direction (ρu_x) with x. Clearly, closer to the surface, mass flow decreases with x near the leading edge and remains relatively constant inside the flame with x. This can be expected from the gas temperature profile, which increases with x near the leading edge and remains relatively constant inside the flame as shown by the green lines in Figure 15. On the other hand, far from the surface, the mass flow in x-direction increases with x as one approaches the flame and then drops rapidly with x before leveling off inside the flame.

The effects of expansion are most apparent on the y component of the velocity uy, which are displayed in Figures 16. Near the leading edge region of the porous plate, the HRR_v is the largest and the contour begins to turn parallel to the plate with distance along the surface. Therefore, the y component of the expansion flow increases as the HRR_v contour begins to turn toward parallel. The velocity u_y is nearly zero in the combustion zone, where maximum heat is generated. Below that zone, u_y is negative and is small due to blockage by the wall. Above that zone, u_y increases with y to a maximum and then decreases. Based on continuity equation, as u_y begins to decrease with y, u_x must increase with x as indicated by red region in u_x contour map shown in Figure 12. Farther from the leading edge, the HRR_v contour becomes more parallel to the plate but the magnitude of HRR_v reduces sharply resulting in very small expansion flow in the y direction. Figure 17 shows quantitatively that the y component velocity increases with x near the leading edge region and farther from the surface and then decreases with x as the expansion effects die out. The increase in u_y is large up to 15 cm/sec compared to its value at the porous surface. Figure 18 shows that u_y increases with y at smaller values of y due to the expansion effect. At larger values of y, u_y decreases with y as the expansion effects die out in the bulk flow. Figure 19 shows mass flow in the y direction (ρu_y) along the plate x. Like u_y profiles, (ρu_y) shows an increase in the y direction flow near the leading edge at distances far from the surface due to the expansion effects. At large distances from the leading edge, the y direction mass flow decreases to very small values inside the flame as the temperature reach relatively constant values.

The interaction among various effects govern the velocity profiles and are very complex. Further work is needed to separate the various effects and to determine precisely different parameters that control the fluid dynamics generated by the presence of the flame.
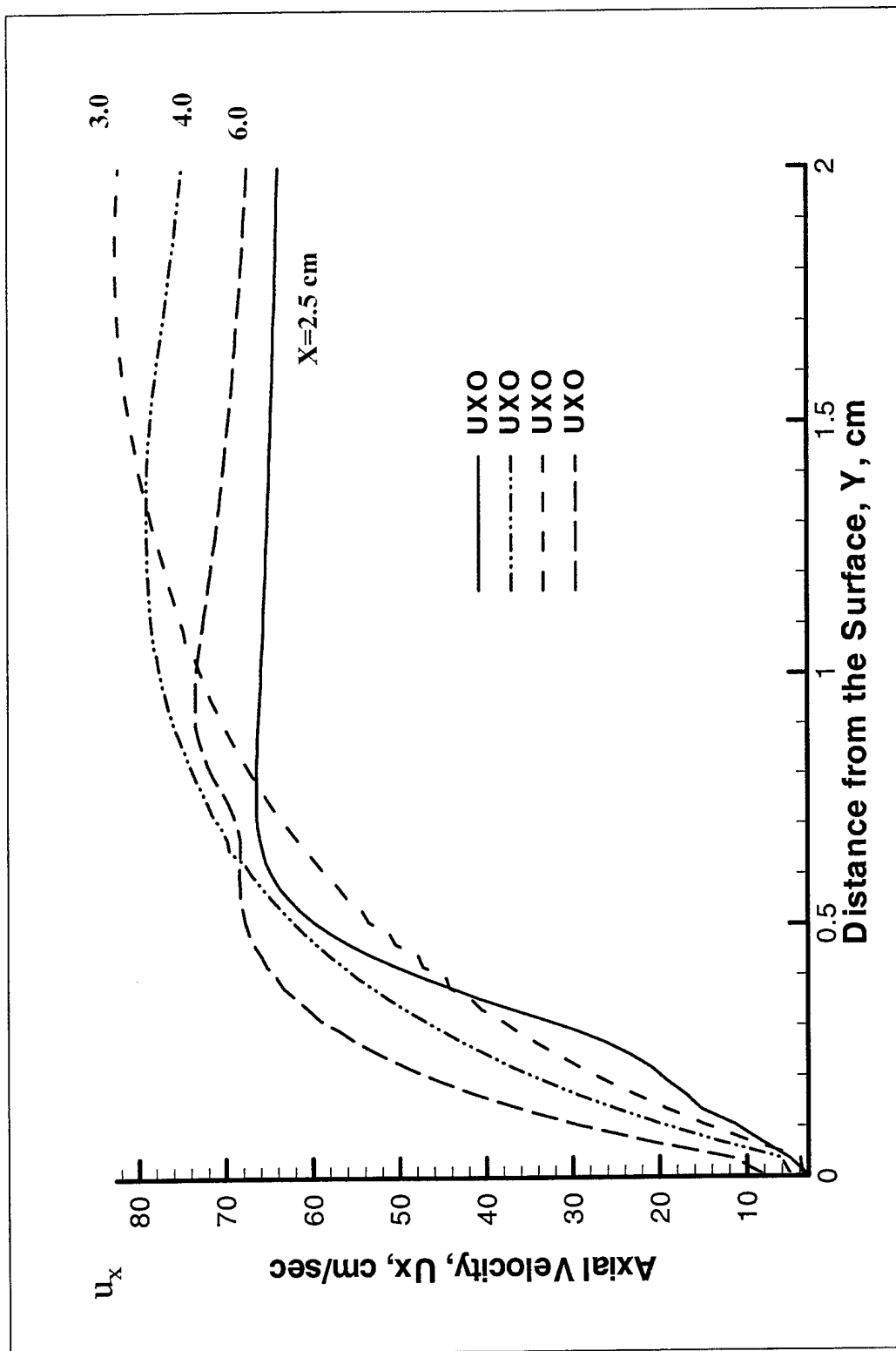
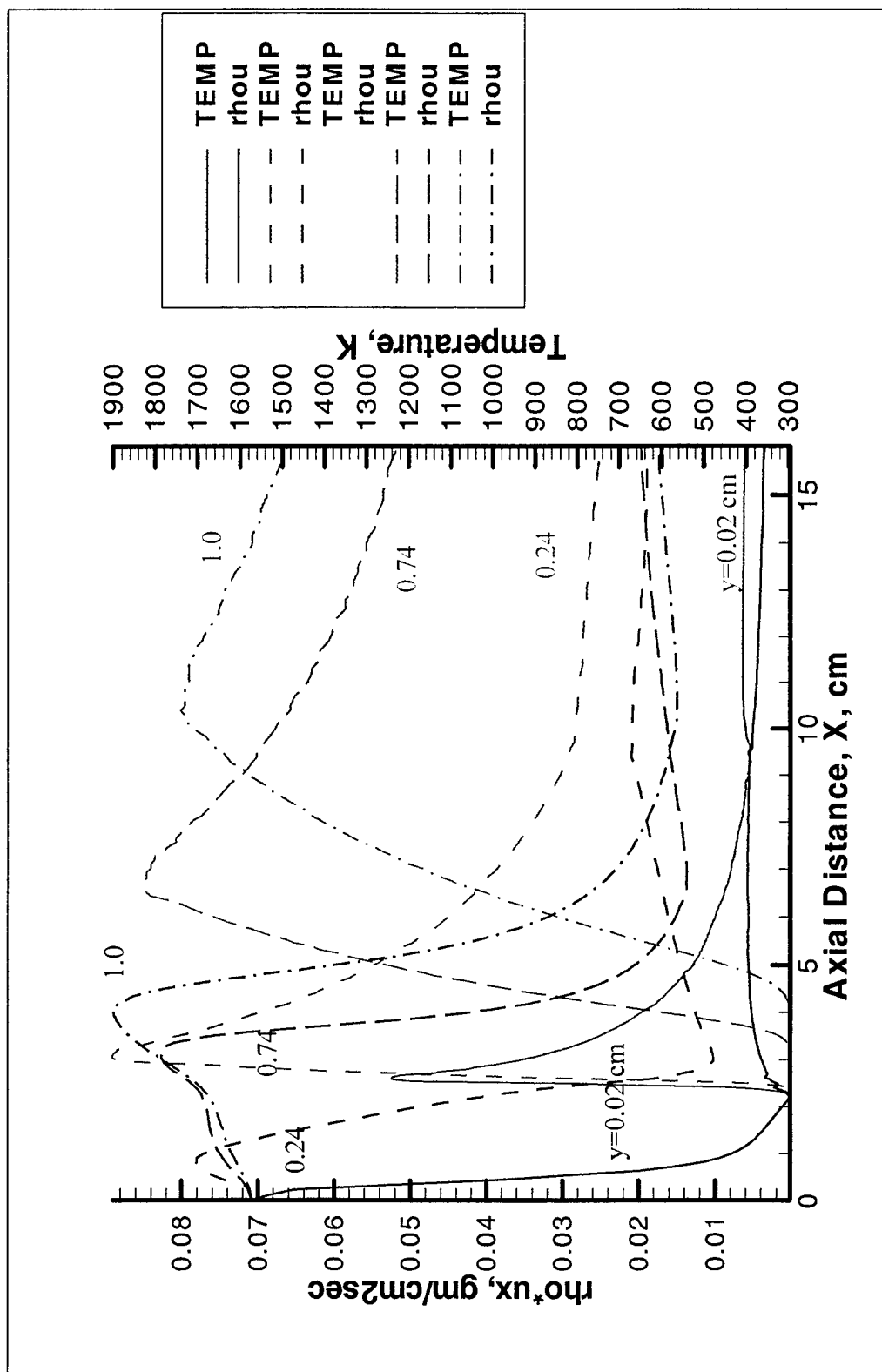Figure 14   Axial velocity (u_x, cm/sec) with distance from the surface, y

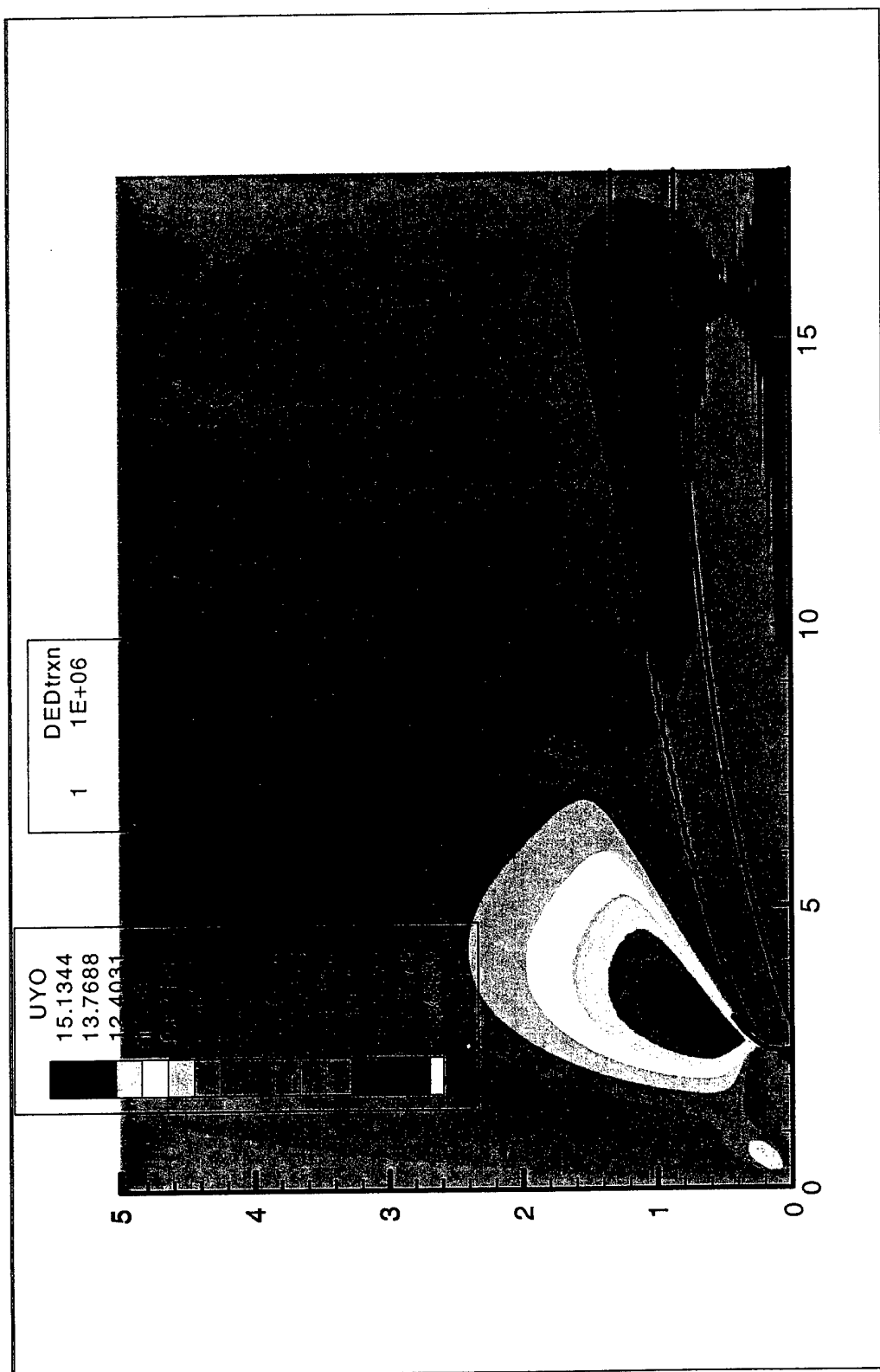Figure 15   Axial mass flow (gm/cm²sec) are in red, and temperature (K) are in green with axial distance x

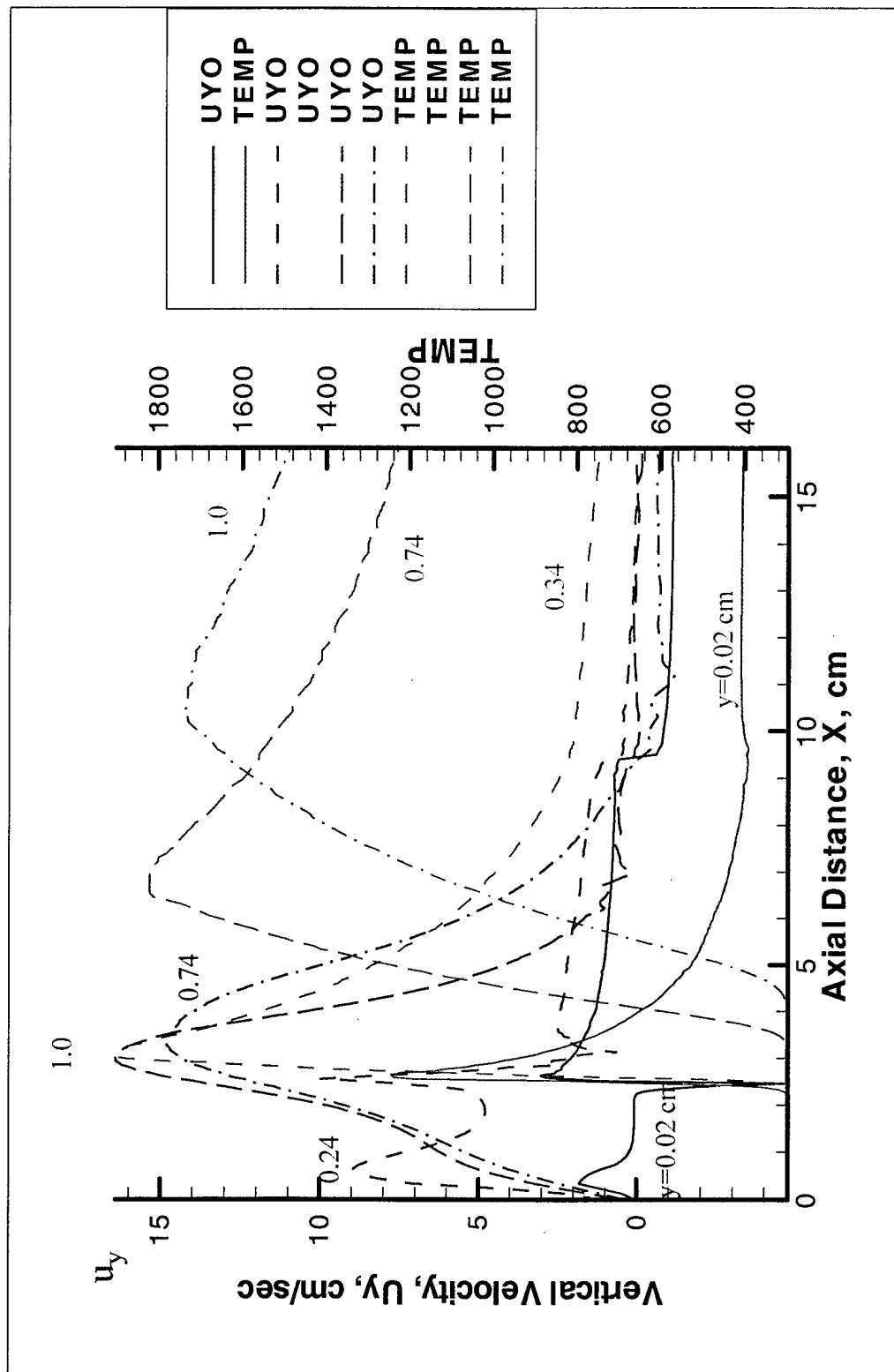Figure 16 Vertical velocity (u_x, cm/sec) contours along with a contour of heat release rate

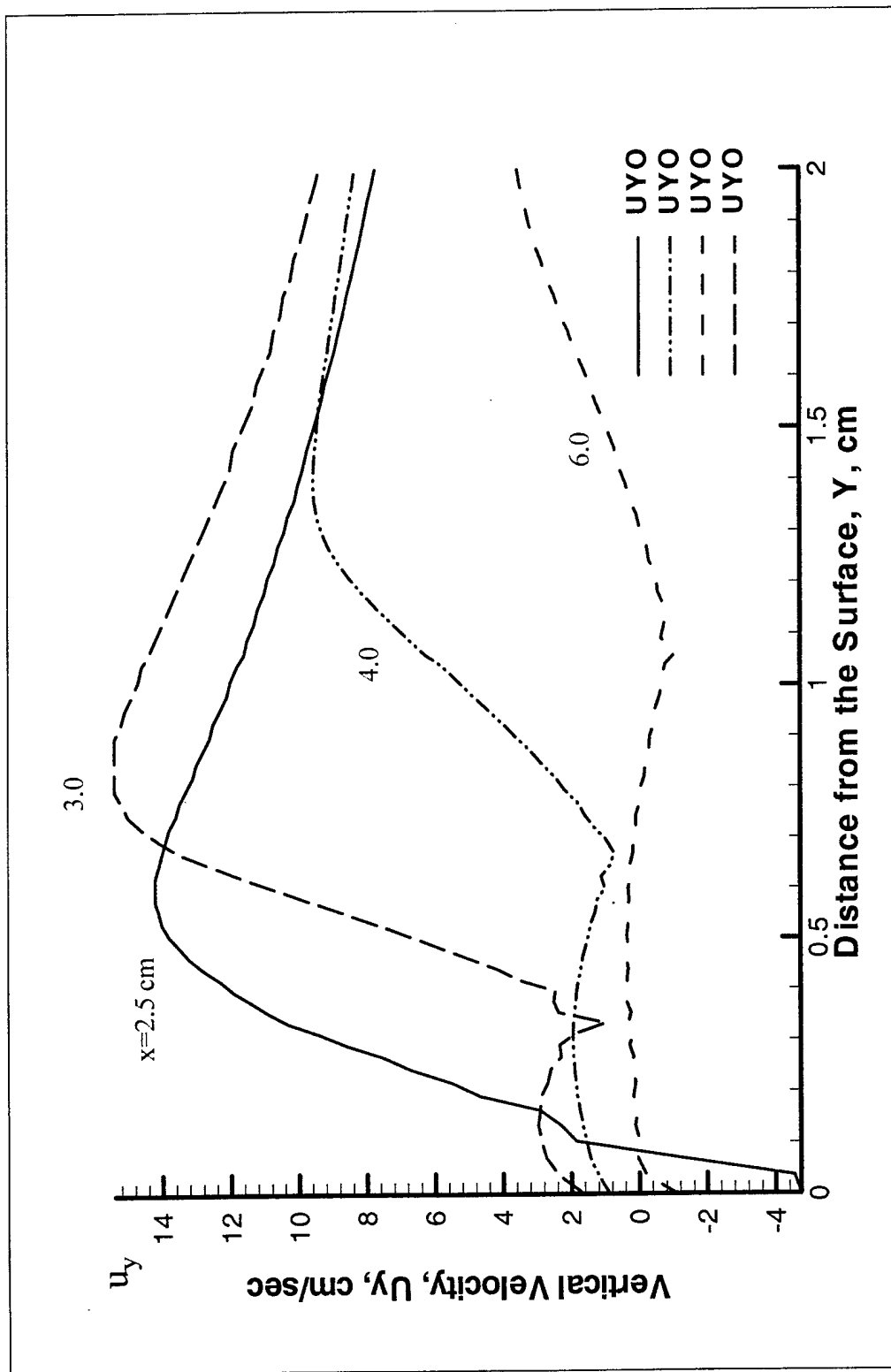Figure 17   Vertical velocity (u_y, cm/sec) profiles with x

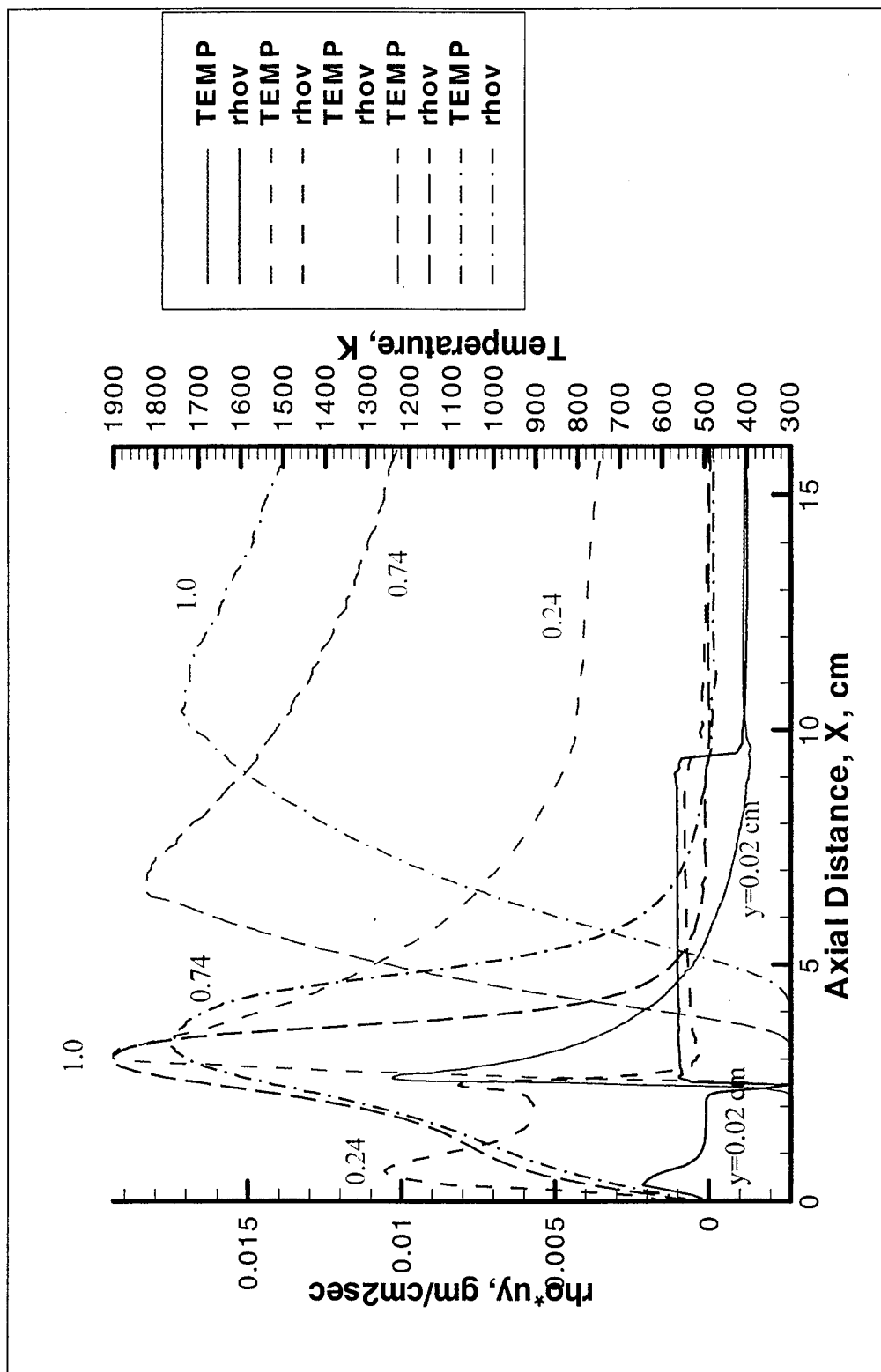Figure 18   Verical velocity (u_y, cm/sec) profiles with y

Vertical mass flow (gm/cm²sec) profiles with x

Figure 19

5.2.3 Specie Concentration Profiles

The fuel ejected from the solid surface travels toward the reaction zone, where it diffuses and mixes with oxygen and reacts to produce products. As it approaches the reaction zone, it also gets heated up to the flame temperature. As the temperature rises the gases expand and density as well as specie concentrations decrease. Thus the concentration profiles are the result of convection of air and fuel from the surface, diffusion, reaction, and expansion of gases. Figure 20 shows n-pentane concentrations contours along with the HRR_v contour displayed in black. One can see that the fuel concentrations are at least three orders of magnitude lower in the region inside the heat release rate contour, where reaction consumes the fuel, than at the surface of the solid. The steep drop in concentration is mostly due to the consumption by the reaction and to some extent due to expansion associated with increased temperature. Oxygen concentrations also exhibit similar drop in concentrations in the reaction zone as displayed in Figure 21. Oxygen also undergoes expansion and diffuses into the flame zone, where it is consumed by the reaction. Nitrogen, on the other hand, exhibits a different profile since it is not affected by the reaction. Its concentrations are displayed in Figure 22 and are affected only by diffusion and expansion. The expansion effect can be seen clearly in the nitrogen concentrations, which drops by a factor of about 7 in the reaction zone. Figure 22 also shows that nitrogen concentration is higher near the surface than near the flame due to lower temperature at the surface than in the flame. Figure 23 and 24 show concentration contours of CO_2 and H_2O respectively along with the HRR_v contour. One can see clearly that the product concentrations are higher near the solid surface than inside the reaction zone, where they are generated. This is clearly the manifestation of the expansion effect, which is much higher in the reaction zone than near the surface due to lower temperature at the surface.

The gas expansion due to combustion affects specie densities to a much greater degree that it affects the specie mole fractions. This can be seen by dividing both sides of the equation (5) by total number density, C_{tot} and replacing the concentrations by mole fractions in the entire equation except in the reaction term, W_k/C_{tot}. This results in

$$\frac{\partial X_k}{\partial t} + \frac{\partial u X_k}{\partial x} + \frac{\partial v X_k}{\partial y} = \frac{\partial V_{dk} X_k}{\partial x} + \frac{\partial V_{dk} X_k}{\partial y} + \frac{W_i}{\sum_i C_i} , \qquad (53)$$

and

$$\frac{W_i}{\sum_i C_i} = k_c X_i . \qquad (54)$$

For a first order reaction, the rate constant, k_c, given by equation (31) is independent of C_k. For n-pentane, however, the rate constant depends on specie density raised to the power 0.75. Therefore, expansion reduces density and tends to reduce the rate constant, while the Arhenius
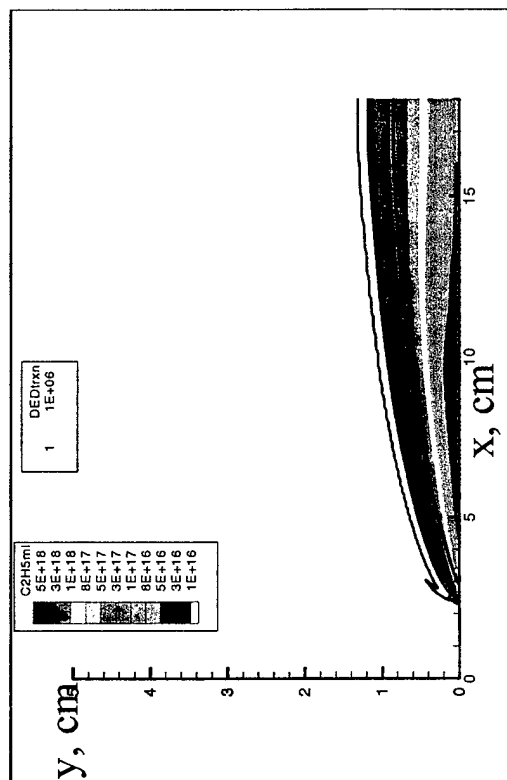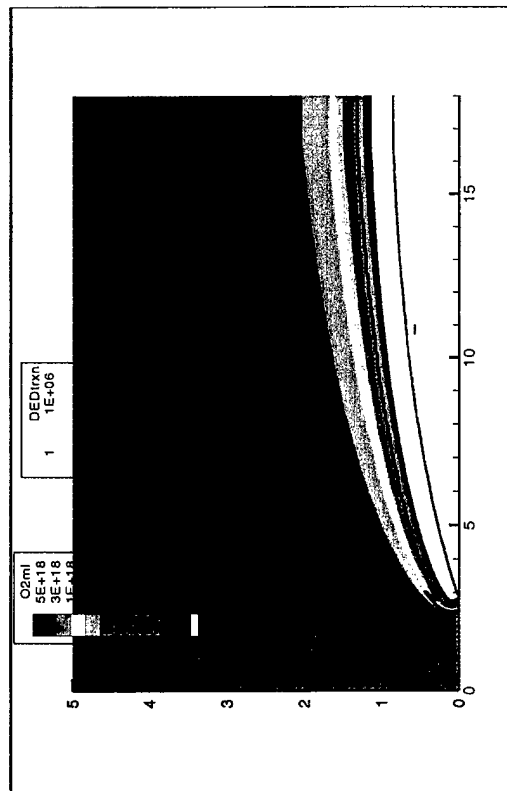
Figure 20   n-Pentane (#molecules/cm³) Profiles
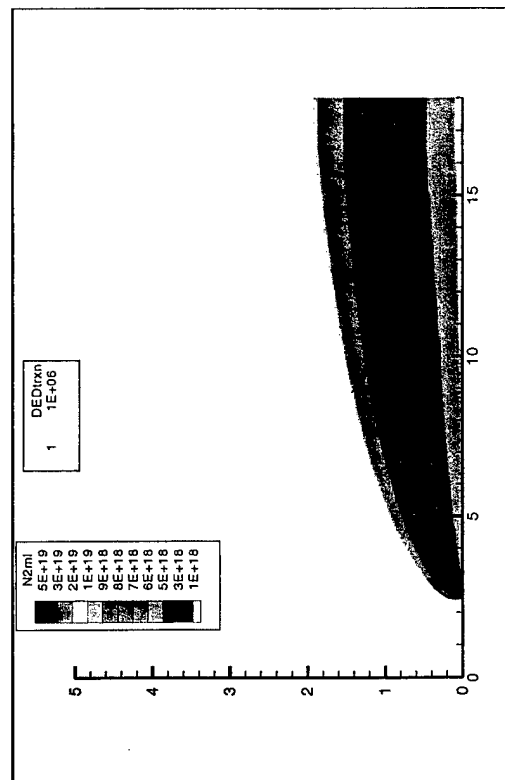
Figure 21   Oxygen (#molecules/cm³) Profiles
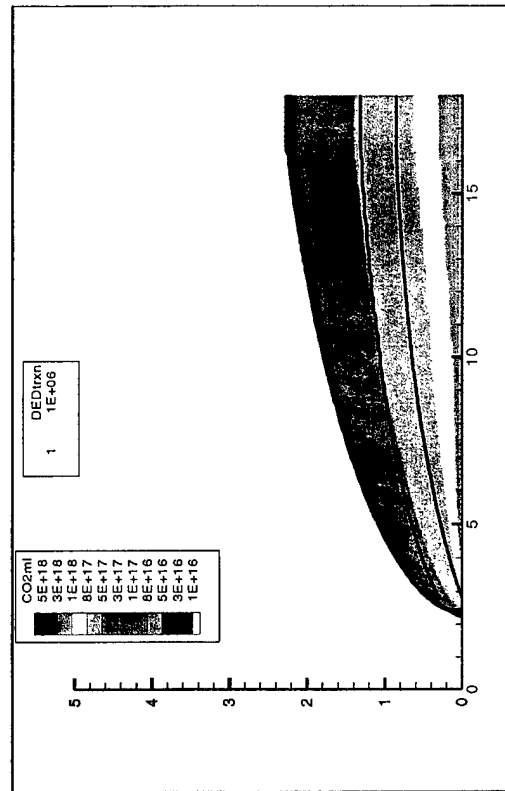
Figure 22   Nitrogen (#molecules/cm³) Profiles

Figure 23   Carbon Dioxide (#molecules/cm³) Profiles

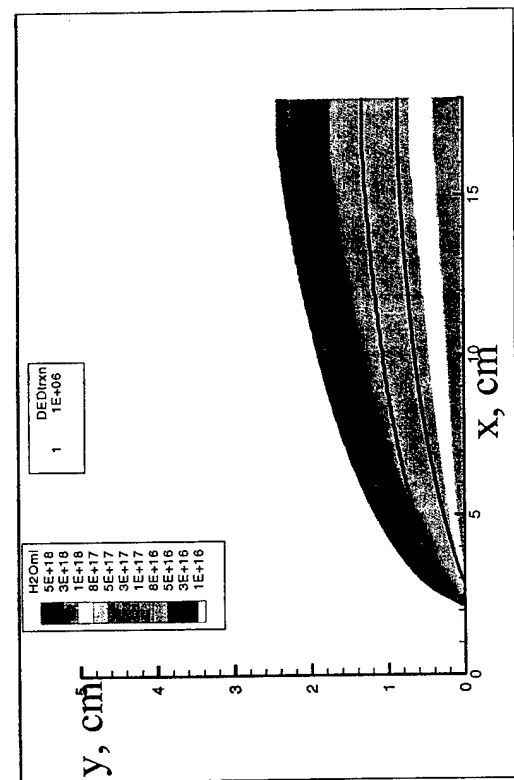Figure 25 n-Pentane Mole Fraction Profiles

Figure 27 CO_2 Mole Fraction Profiles

Figure 24 Water Vapor Profiles, #molecules/cm^3
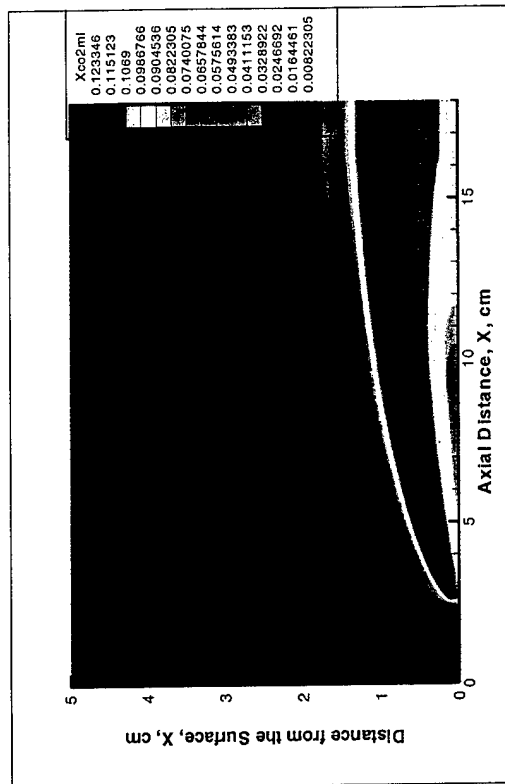
Figure 26 N_2 Mole Fraction Profiles

effect tends to increase the rate constant exponentially. Thus the expansion effect on the rate constant and the specie mole fraction is not significant compared to the Arrhenius effect.

Figures 25 shows mole fraction contours of fuel and are similar to the concentration contours displayed in Figures 20. The oxygen mole fractions were also found to be similar to its concentration contour shown in Figure 21. However, one notices that the change in mole fractions from their values in the bulk to the reaction zone are smaller than corresponding change in specie densities. Figure 26 shows that the nitrogen mole fraction is lowest near the surface where fuel is injected unlike the concentration contours shown in Figure 22, which is affected by the gas expansion. Figures 27 displays CO_2 mole fraction contours. Unlike the concentration contours displayed in Figure 23, they show a maximum in the flame zone, where they are generated. Water vapor mole fractions were found to be very similar to the CO_2 mole fractions. A comparison of mole fraction profiles with the specie density profiles shows the gas expansion effects.

In order to gain quantitative understanding, we have plotted mole fractions of O_2, fuel, and N_2 together in Figures 28. Here, x and y values represent distance in axial and vertical directions respectively. The leading edge of the porous plate through which fuel is injected uniformly extends from x=2.45 cm to 9.5 cm. Left of the leading edge is occupied by pure air and the right of the leading edge is occupied by combustion gases. Figure 28 shows O_2 concentration profiles decrease to near zero followed by increasing fuel concentration profiles along the porous plate as a result of combustion reaction. The flame is located in the overlap region, wherein the O_2 decreases to zero and fuel concentration begins to increase from zero. Near the surface (y=0.02 cm), the oxygen profiles are very steep with axial distance due to high reaction rates due to very small flame stand off distance. The fuel mole fraction increases from 0 near the leading edge to 0.45 near the trailing edge of the porous plate due to fuel injection and then decreases along the surface of the non-porous plate. Away from the surface (y=0.74 cm), the oxygen profiles become less steep with x due to decreased reaction rates and increased flame standoff distance. Also, away from the surface, fuel convection from the plate becomes less significant relative to diffusion, and the fuel mole fraction increases continuously all the way to the end of the channel. Nitrogen, however, exhibits a reverse trend. It decreases along the porous plate due to fuel injection and increases along the non-porous plate in the region close to the surface. Away from the surface, nitrogen decreases continuously all the way to the end of the channel.

Figure 29 shows the specie profiles along vertical distance from the surface, y. Figure 29 shows clearly that the fuel diffuses away from the surface while nitrogen diffuses to the surface as indicated by negative and positive gradients at the surface. The boundary condition, which is given by equation (41), requires that the sum of the diffusive and convective flux be equal to the fuel injection rate per unit area. The boundary condition for nitrogen requires that the diffusive and convective fluxes are equal and opposite such that the sum is zero. Thus, no net flux of nitrogen is imposed along the surface. On the non-porous section of the surface (x=14 cm, y=0), there is no convective flux. Therefore, the diffusive flux approaches zero as indicated by the zero gradients at the surface. Fuel concentrations decrease, oxygen and nitrogen concentrations increase with distance from the surface. The flame is located at positions, where the fuel concentration approaches zero and oxygen concentration begins to rise. Figure 29 shows a
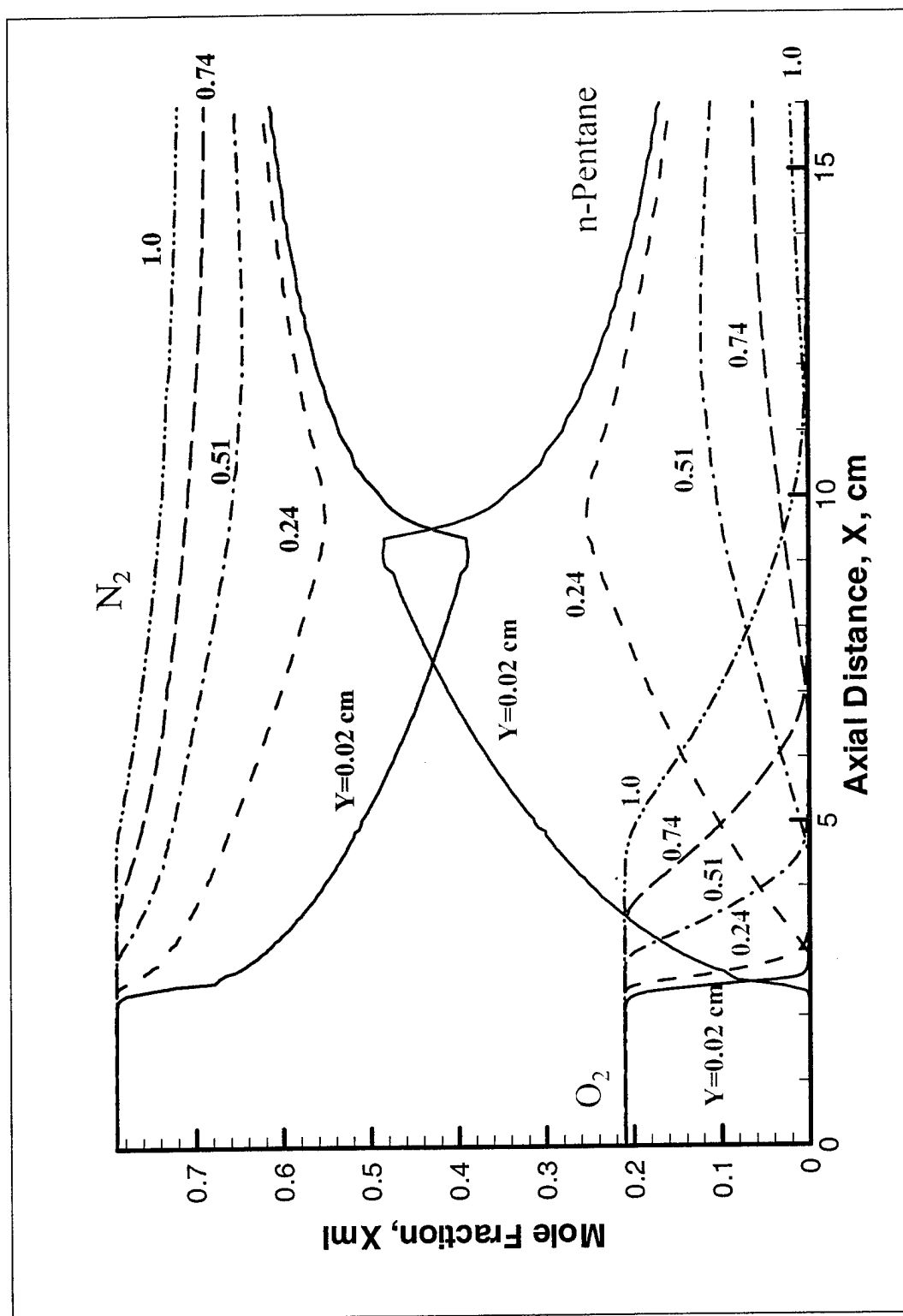
44

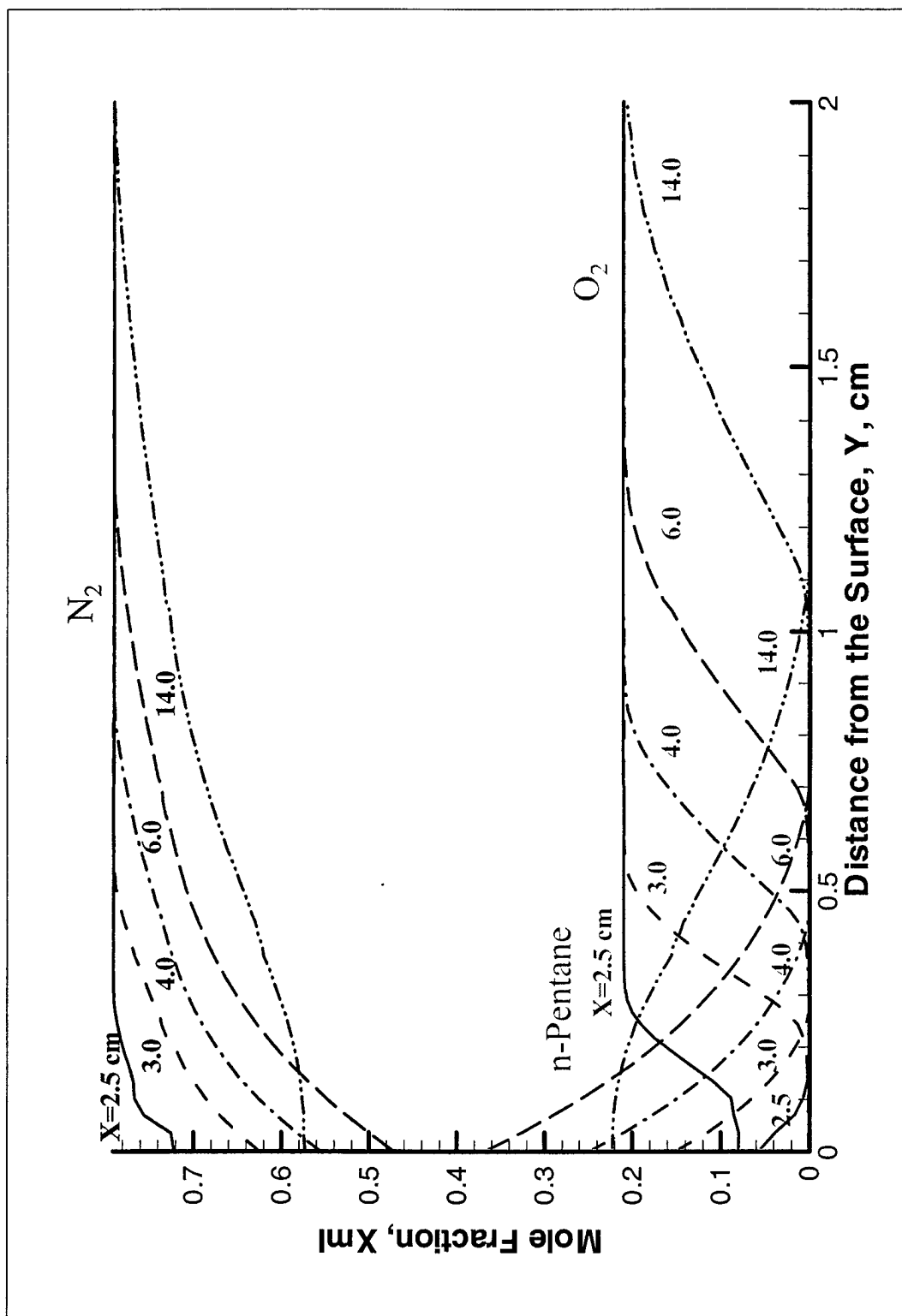Figure 28   Mole Fraction Profiles of O_2, N_2, n-Pentane Along Axial Distance, x

Figure 29   Mole Fraction Profiles of O_2, N_2, n-Pentane Along Vertical distance, y

significant mixing zone near the leading edge (x=2.45 cm) where both oxygen and fuel are present in significant concentrations. This overlap zone gets very thin and the concentrations in the mixing zone become very small as x increases from the leading edge. Also, the concentration profiles get more flat at larger distances from the leading edge of the porous plate. Near the surface (y<2 mm), the fuel concentration increases along the porous plate and then decreases along the non-porous plate due to the convective effect of injection.

Figure 30 shows product concentration profiles together. Water and CO_2 have similar profiles as expected. Following stoichiometry, slightly more (6/5 moles of H_2O per mole of CO_2) H_2O is generated than CO_2. The difference in diffusivities contribute to the difference in the profiles. The products are produced in the flame, which is located near the maxima exhibited by the profiles. Near the surface, the product concentration increases steeply in the reaction zone and then decreases along the porous plate as the fuel ejected from the surface dilutes the products until the trailing edge of the porous plate. The product concentrations then increase along the non-porous plate. Away from the surface, where the fuel convection from the surface is less significant, the product concentration decreases continuously all the way to the end of the channel. One also notices that the rise in product concentration becomes less steep as one moves away from the surface due to the reduced reaction rates and flame standoff distance increases with x.

Figure 31 shows product concentration profiles along the vertical distance, y, from the surface. Again, the flame is located at the maxima of product profiles. The products diffuse away from the flame zone to the surface as indicated by the positive gradient at the surface. The surface boundary condition requires that the diffusive and convective fluxes be equal and opposite such that the sum is zero representing no net flux of products at the surface. On the non-porous surface (x=14 cm, y=0), no convective flux exists. Therefore, the diffusive flux approaches zero as indicated by the zero gradients at the surface. The mole fractions of water vapor are slightly higher than that of CO_2 except in the flame zone, where they are about equal at distances away from the leading edge. The difference between CO_2 and H_2O concentrations seem to increase with distance along the plate outside the reaction zone.

In order to show the characteristics of the "reaction zone" clearly, in Figure 32, we have plotted all of the specie mole fractions, temperature, and HRR_v with y, and at about 1.5 cm distance from the leading edge (x=3.95 cm) of the porous plate. One can see that peak temperature and energy are released near the position, where the oxygen and fuel mole fractions are low and the profile cross one another (about stochiometric) in a thin region. The heat is released within this thin region.

5.2.4 Surface Concentration of Fuel and Heat Feedback

The concentration of species at the surface are determined by the surface boundary conditions given by equations (42) and (43). They show that the sum of diffusive and convective mass flux be a constant. Therefore, the convective flux must increase with distance along the surface x, since diffusive flux decreases with x due to increasing flame standoff distance. Figure 33 shows specie mole fractions at the surface with axial distance. It shows that the fuel mole
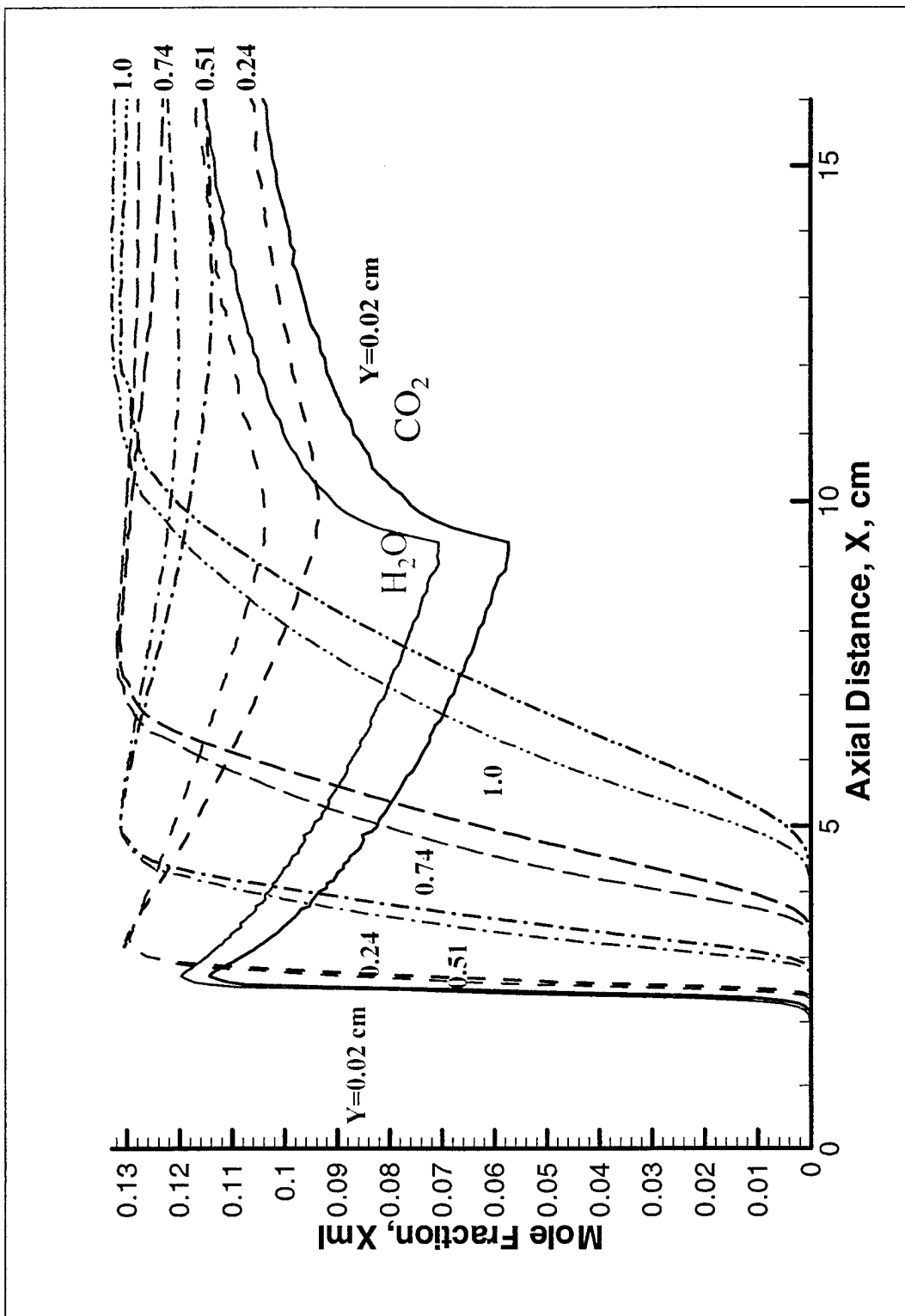
Figure 30   Mole Fraction Profiles of CO_2, H_2O Along Axial Distance, x

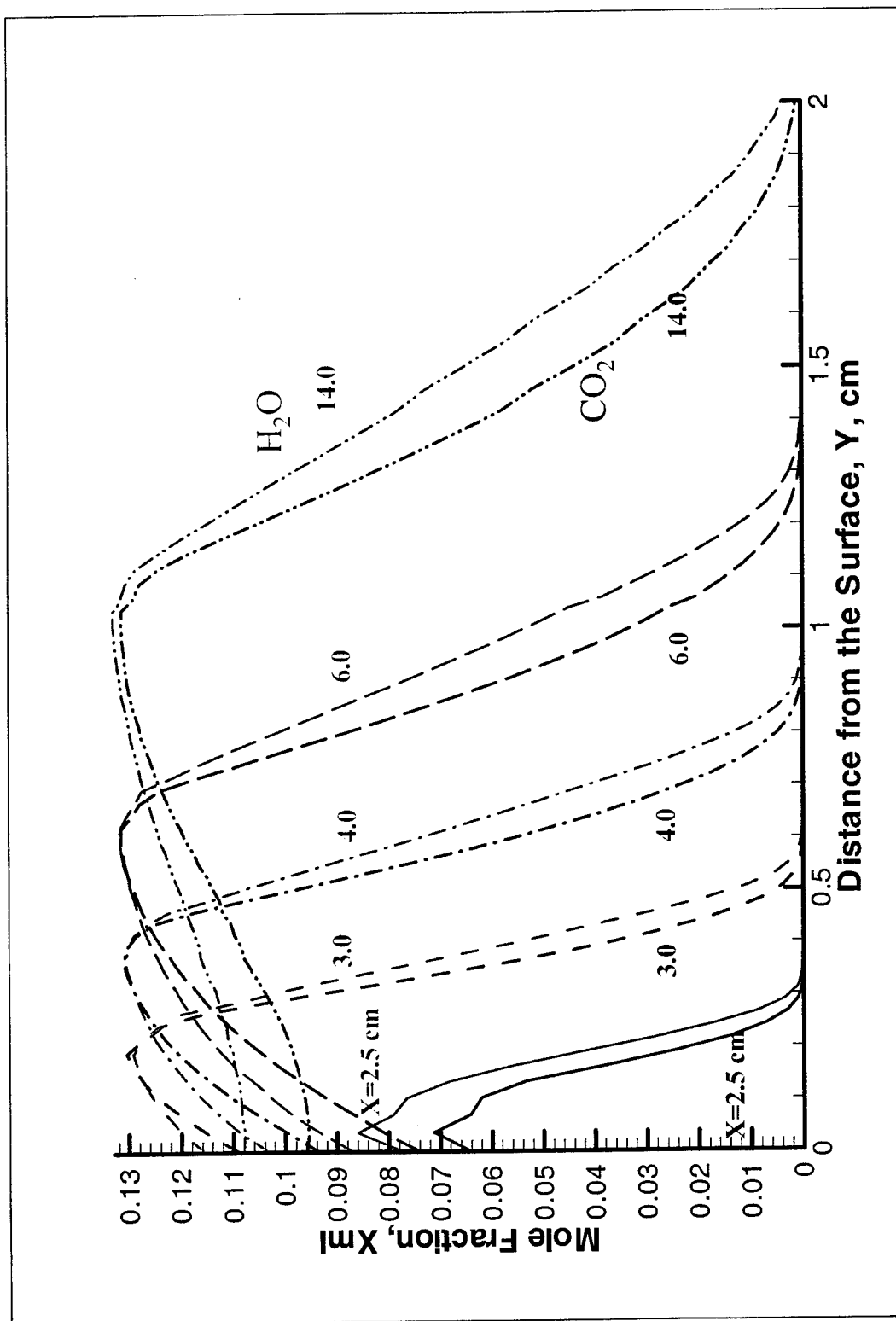Figure 31   Mole Fraction Profiles of CO_2, H_2O Along Vertical Distance, y
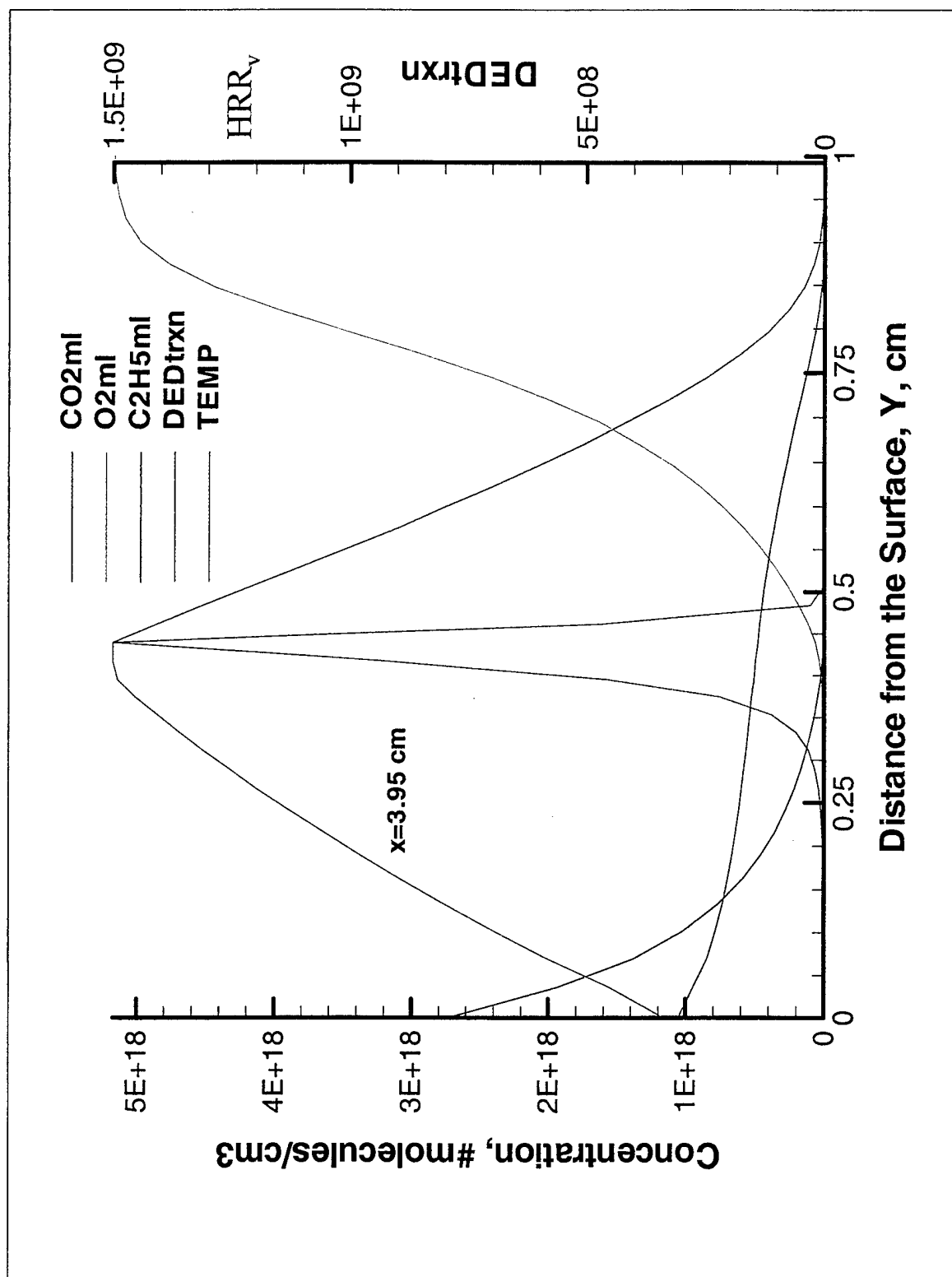
49

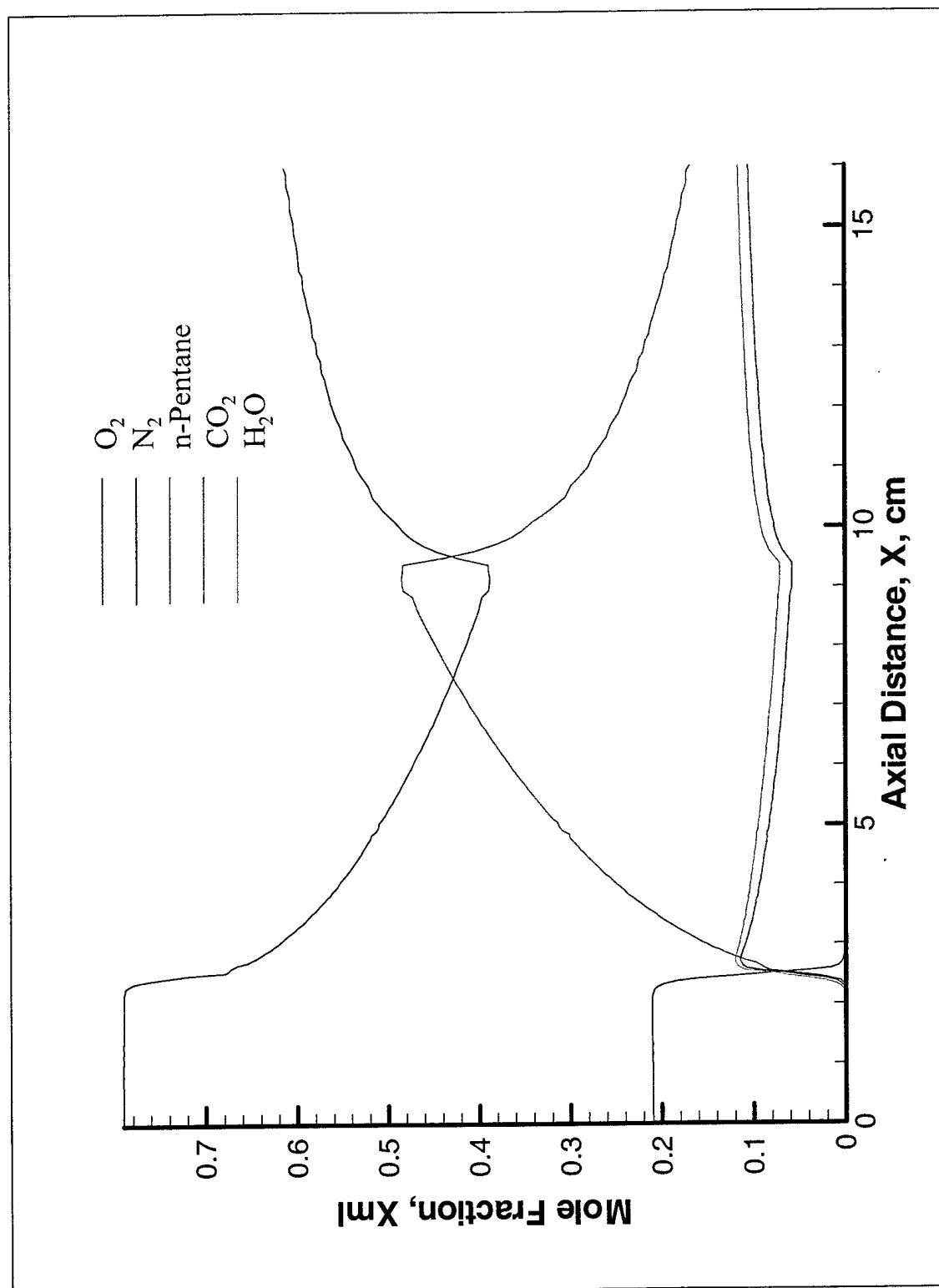Figure 32   Reaction Zone Profiles: fuel, oxygen, product, temperature, and heat release rate

Figure 33   Surface Mole Fraction Profiles

fraction is the lowest near the leading edge (x=2.5 cm) of the porous plate, where the flame is the closest to the surface and diffusive flux is high. As the distance from the leading edge increases, the fuel mole fraction increases due to increased standoff distance and decreasing diffusive fuel flux. At the trailing end of the fuel plate, the fuel mole fraction ($X_{k=1}$=0.48) is still less than one, showing significant fuel diffusion to the flame zone. Along the non-porous section, following the porous section, the fuel mole fraction begins to decrease as there is no fresh fuel available to compensate for its consumption by the reaction. The reaction rates are high near the leading edge as indicated by the steep decrease in oxygen mole fraction and high mole fractions of CO_2 and H_2O. The reaction rates decrease along the porous plate producing products at a decreasing rate with distance. Furthermore, near the porous surface, dilution of gases by fresh fuel ejecting from the surface dominates. This leads to a decrease in product concentrations along the surface even though they are being produced by the reaction. On the non-porous plate following the porous section, the products mole fractions begin to increase in the absence of the fuel dilution effect. A very similar trend is exhibited by the nitrogen profile, which shows a decrease along the porous plate due to fuel dilution effect followed by an increase along the non-porous section.

The surface temperature is determined by the energy balance at the surface given by equation (44), which states that the energy q_w, feedback to the surface from the flame is equal to energy lost through the back of the porous plate to the ambient. Note that both the surface temperature and surface heat flux q_w vary along the plate and are calculated as a part of the solution, once the heat transfer coefficient h_w is specified. Figure 34 shows that the surface temperature and heat flux increase rapidly with distance x, near the leading edge of the plate, where the flame is closest to the surface. This is the heat up region where the reaction rate, convective transport of the reactants and heat loss through the plate are expected to play a crucial role in determining the surface temperature. This region, where flame standoff distance is at the minimum, is also been referred to as "flame attachment" in the literature (This term "flame attachment" is misleading since flame does not really attach to the surface unless there is combustion on the surface at a high temperature). This leading edge region is followed by a boundary layer region, where the surface temperature and the heat flux decrease with axial distance as the flame standoff distance increases. The surface flux is proportional to surface temperature as specified in equation (44). Figure 34 shows that the peak heat flux is several times higher than that at the end of the porous plate for h_w=6.92e04 ergs/cm^{2}sec. The surface temperature is also much higher than at the trailing edge of the porous plate. One should keep in mind that this profile is a function of various parameters and will be discussed in a separate report.

Figure 35 shows a power law fit to the Navier-Stokes solutions for the heat flux at the solid surface. The fit is not perfect, since, as expected, the power law may apply only at some distance from the leading edge, which is represented as x_s=x-L_1=0 in Figure 35. Extrapolation of the power law to the leading edge yields infinite surface flux. An exponent of -0.7 seems to fit the solution at large values of x_s. Based on boundary layer theory, such as in the solution to "Emmons problem", the surface heat flux is expected to decrease as 1/sqrt(x_s). A power law fit with an exponent close to -0.5 is shown in Figure 36. The square root does not fit the computations to a significant degree. The square root exponent seems to apply close to the leading edge. As x_s increases the exponent decreases and approaches -1.0 at x_s>5 cm. This is surprising since the square root exponent is expected to apply farther from the leading edge based
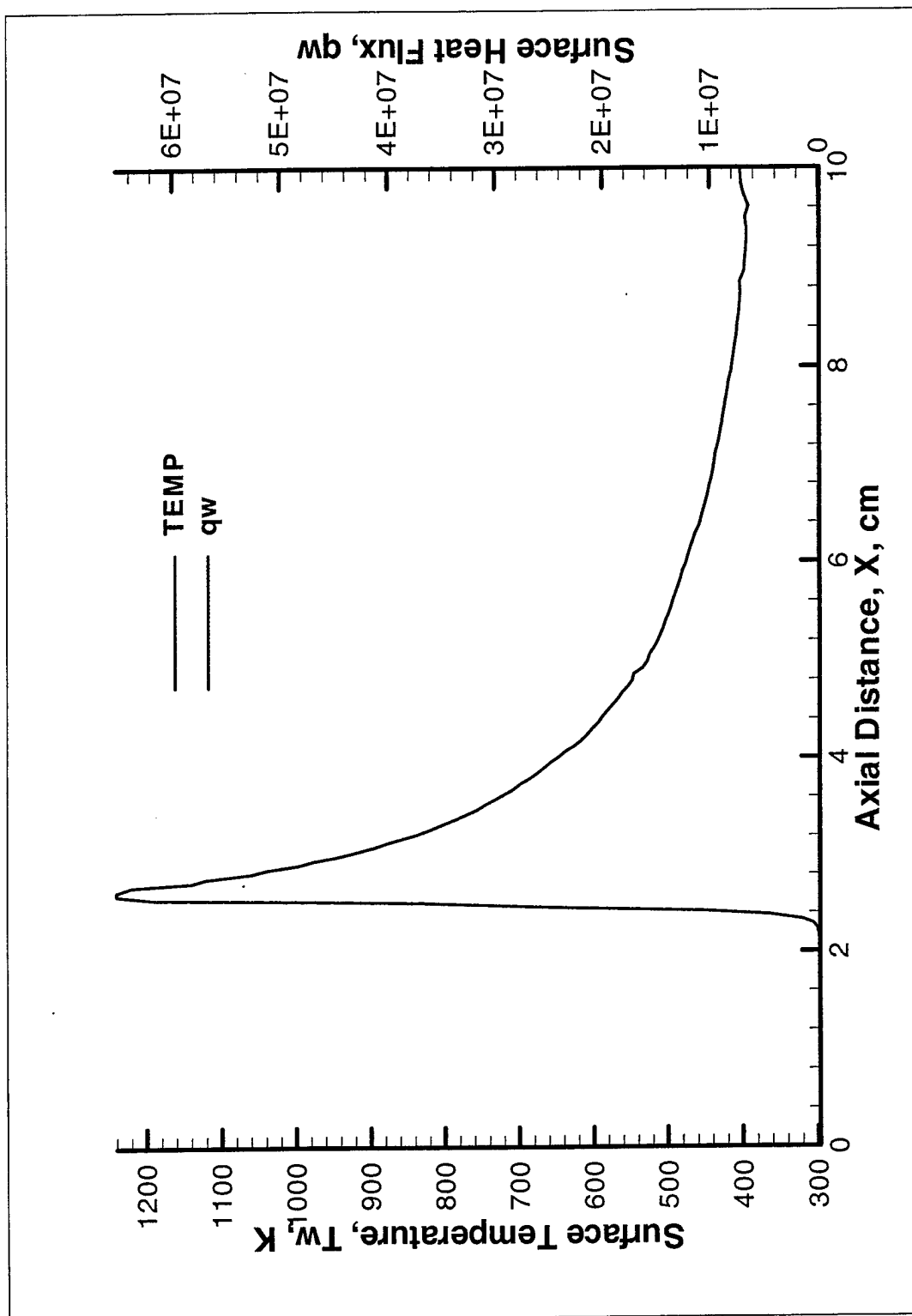
Surface Temperature and Heat Flux Profile

Figure 34

$$q_w = \frac{2.86 \times 10^7}{x_s^{0.70}}$$

O NS Solutions

— Power Law Fit

Distance from the leading edge, Xs, cm

Surface heat flux, qw
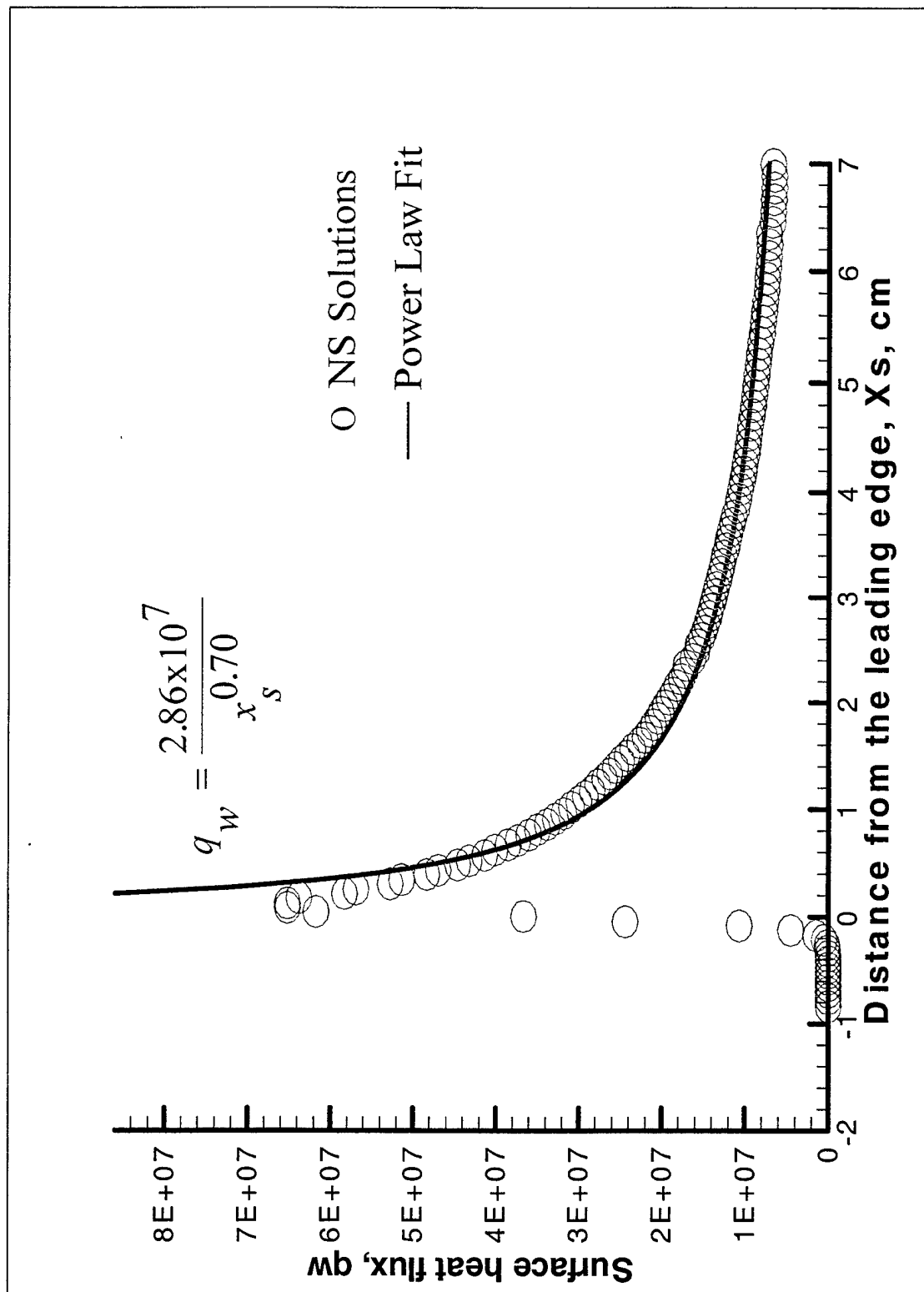
Figure 35   Power law curve fit to surface heat flux profile with x_s

$$q_w = \frac{3.0 \times 10^7}{x_s^{0.51}}$$

O NS Solutions

— Power Law Fit

Distance from the leading edge, Xs, cm
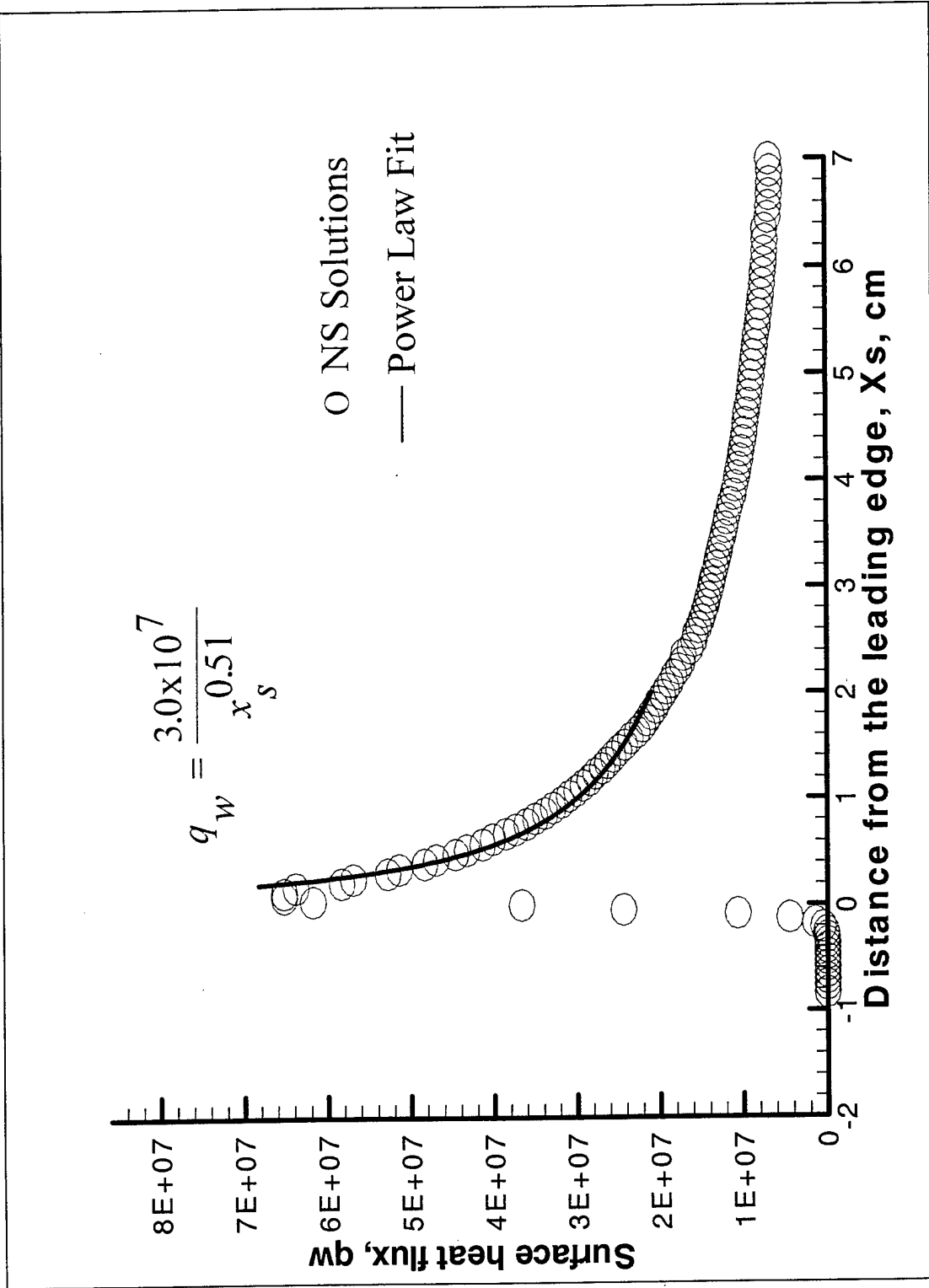
Surface heat flux, qw

Figure 36   Power law curve fit to surface heat flux

on boundary layer theory. In any case, it is clear that a power law model or a boundary layer model can not adequately represent the wall heat flux profile along the entire length, from leading edge to the trailing edge, of the plate. However, our computations suggest an exponent of 0.7, which is higher than that suggested by Emmons (1956), fits the right arm of the heat flux profile. One must note the mass loss rate in Emmons' analysis is proportional to the surface heat flux and decreases as 1/sqrt(x_s), unlike the present problem, where the mass injection rate through the plate is uniform along the plate. Also, Emmons assumed specie independent properties, which were shown to have significant effect by Kikkawa et al. (1973).

Similarly, the fuel mole fraction at the surface can also be fitted with a power law and is shown in Figure 37. This yields an exponent close to one half (0.447) and clearly fits well to the full Navier-Stoke solutions for the entire length of the plate. Near the leading edge, where x_s=0, the profiles are very steep and may be fitted with a combination of exponential function and a power law. However, a further analysis based on theoretical grounds is needed.

The heat feedback from the flame to the solid surface is a crucial quantity of interest in burning of solids, since it drives the solid pyrolysis. The mass loss rate in burning solids is closely related to the heat feedback. The heat flux at the surface given in Figure 34 can be integrated along the plate length to obtain the heat feedback and is given by the following equation;

$$Q_b = \frac{\int_0^{x_i} q_w dx_s}{\int_0^L q_w dx_s} (100) , \qquad (55)$$

where Q_b is the % of heat feedback, x_s is distance from the leading edge of the porous plate, and L is the total length of the porous plate. The heat feedback Q_b, (ergs/sec) is shown in Figure 38 along with the local heat flux q_w against x_s/L, dimensionless distance from the leading edge of the porous plate. Q_b is zero at the leading edge of the porous plate and increases with distance to 100 % at the end of the porous plate. Figure 38 shows clearly that the first 25% of the porous plate receives about 50% of the total heat from the flame, first 50% of the length receives about 75% of the total heat, and first 75% of the length receives close to 90% of the total heat feedback. Furthermore, the leading edge region, which falls within the first 10% of the length of the plate, receives a significant amount (as much as 30%) of the total heat feedback. Therefore, this figure clearly reveals the importance of the leading edge region, which has traditionally been ignored by the boundary layer theories. This means one could not accurately predict the total heat feedback to the surface purely based on the boundary layer region. A comprehensive analysis presented in this work, which accounts for both the leading edge and boundary layer limits, is needed.

6.   CONCLUSIONS

Time-dependent numerical solutions of full Navier-Stokes equations were obtained for boundary layer flames to describe the flame development from the leading edge to steady state

The chart shows surface mole fraction of fuel, X_{ml} (vertical axis, ranging from 0.1 to 0.45) versus distance from the leading edge, X_s, cm (horizontal axis, ranging from 0 to 7).

Legend:
O NS Solutions
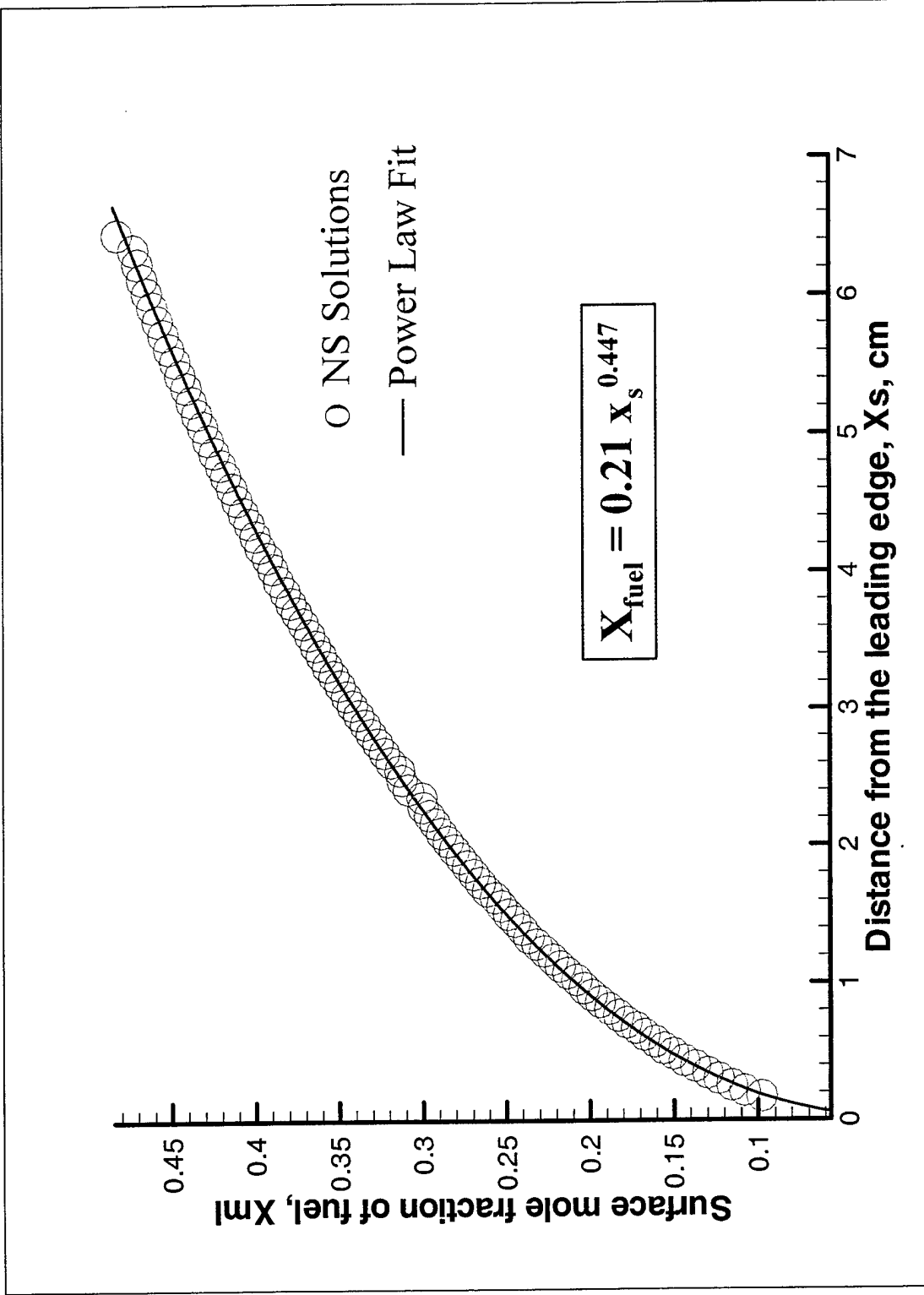— Power Law Fit

$$X_{fuel} = 0.21 \ x_s^{0.447}$$

Figure 37   Power law curve fit to surface mole fraction of fuel

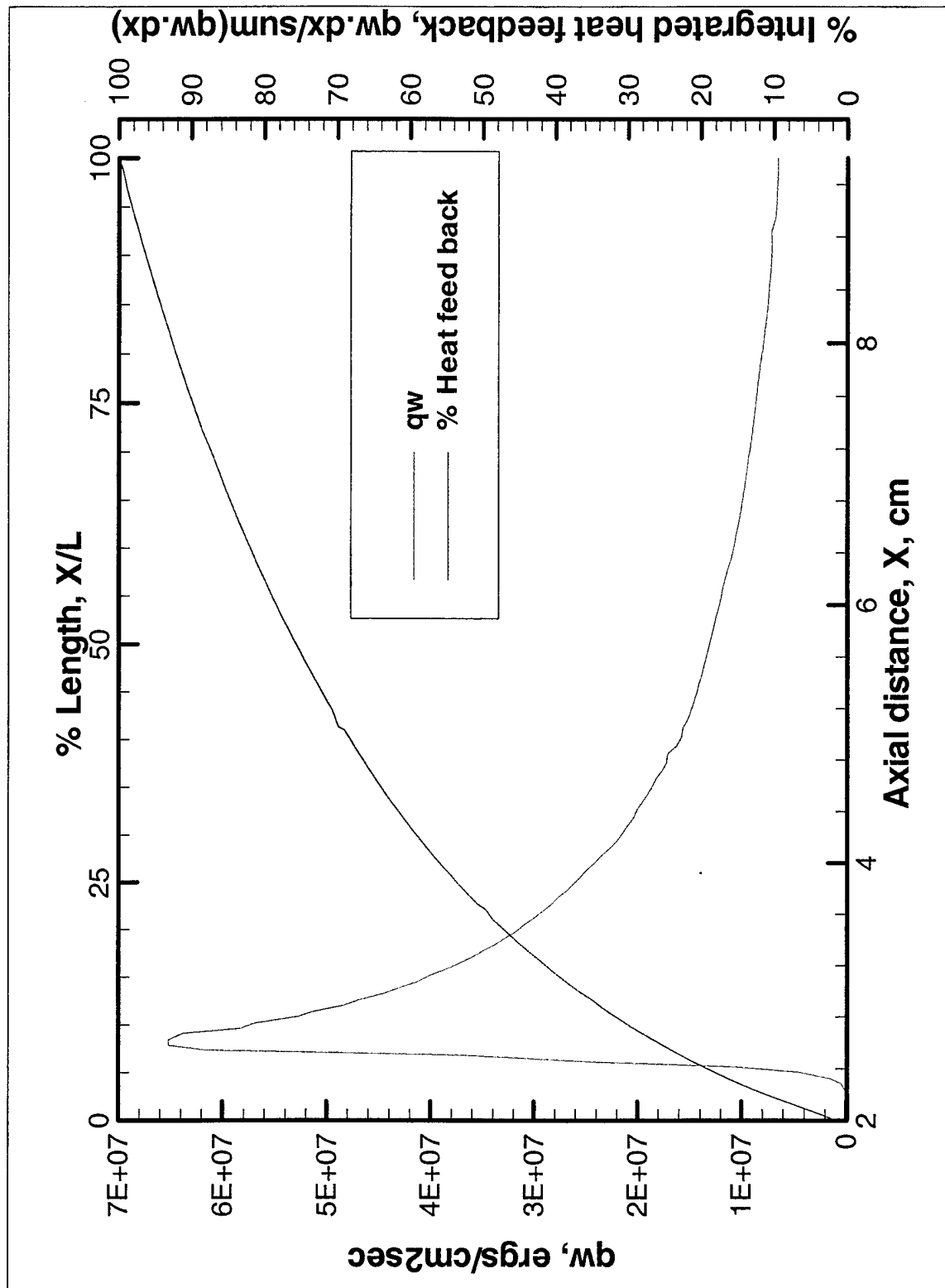Figure 38   Heat flux, q_w, and area integrated heat feed back from flame to the solid surface along the length of the plate

using Barely Implicit Flux-Corrected Transport algorithms for the first time. The solutions for the evolution of temperature and heat release rate (HRR) show the development of an initial triple flame structure, caused by the uniform injection of fuel gas through the plate, into a boundary layer flame at steady state. Uniform injection of fuel along the plate causes formation of a partially mixed gas of fuel and air in front of the advancing flame front. This leads to the formation of a triple flame, which gets weaker with time as the fuel-air mixture gets diluted by the formation of products due to combustion. At the leading edge of the porous plate, however, no triple flame is formed since the leading plate is adiabatic unlike the porous plate. The flame spreads rapidly (1 mm/sec) along the porous plate and slowly (~0.2 mm/sec) along the non-porous section.

Steady-state solutions were obtained for the entire surface that includes both the leading edge and the downstream boundary layer limits for a porous burner for the first time. These solutions are different from those obtained previously for PMMA combustion, where the mass loss rate is not uniform along the solid surface. The steady-state solutions given here show the heat release rate increases steeply near the leading edge, where fresh fuel meets fresh air, and decreases rapidly with distance from the leading edge, x. On the other hand, the flame temperature also increases steeply from inlet air temperature to slightly below the adiabatic flame temperature near the leading edge but decreases slowly with distance from the leading edge due to heat loss from the flame to the bulk of the gas. Peak flame temperatures occur along the peak heat release rate contours.

The velocity field near the leading edge very much influenced by gas expansion due to the density change. As the air approaches the flame zone, its temperature raises rapidly with x (by a factor of $T/T_0=7$) near the outer edge of the flame and then decreases with x only slightly inside the flame. As the temperature rises, density decreases (by a factor of $\rho/\rho_0=1/7$) and mass flux decreases (by about a factor of $\rho u/\rho_0 u_0 =1/5$) near the outer edge of the flame and then remain relatively constant with x inside the flame. This results in an increase in mass flux in the y direction near the outer edge of the flame as dictated by continuity equation (1). The increase in ρv, however, is small compared to that in ρu since $d(\rho v)/d(\rho u)= \delta_f/x$, which is about 1/5. Inside the flame, the vertical mass flux is small and relatively constant. Thus expansion of gases leads to a reduced mass flow inside the flame and an increased mass flow outside the flame. This effect is similar to the effect of drag or no-slip condition (given by equation (12)) on the surface. Drag also decreases the mass flux inside the momentum boundary layer by a large degree, but increases the mass flux outside of the boundary layer to only a small degree due to small boundary layer thickness compared to the axial length. Nevertheless, this increased mass flow just outside the flame leads to maximum in axial velocity profile with distance from the surface and is similar to the experimental observations made by Hirano and Kanno (1973). Hence the maximum in axial velocity profile with y is a combination of the drag and expansion effects rather than due to the presence of an upper wall as interpreted previously by Ramchandra and Raghunandan (1984).

The specie densities for nitrogen and products are found to be the highest near the solid surface and decrease with distance from the surface y. This is mainly due to lower temperature at the surface than in the reaction zone. Indeed, the mole fractions of products, which are not affected much by the gas expansion, show a maximum in the reaction zone as expected.

The surface concentrations of species and temperature are determined by interfacial flux balances using a fixed-point iterative scheme. They vary with position along the surface and time for fixed values of mass injection rate of fuel and heat transfer coefficient for the burner. For uniform injection of fuel gas, which is employed in the experiments on a porous plate burner, the fuel mole fraction increases from zero at the leading edge of the porous plate to 0.45 near the trailing edge. On the other hand, the mole fractions of products and nitrogen are highest near the leading edge and decrease along the porous surface due to the fuel injection and increase along the non-porous section. The surface temperature also decreases with distance from the leading edge as the flame standoff distance increases. The variation in fuel mass fraction along the surface can be fitted to a power law with 0.45 exponent. The variation in specie concentrations and temperature along the surface is much larger than that found in PMMA combustion, where the mass loss rate decreases with distance from the leading edge rather than being uniform.

The heat flux from the flame to the solid surface shows a steep increase near the leading edge followed by a relatively slow decrease with distance from the leading edge of the porous plate. This is in sharp contrast with the previous predictions of boundary layer theories, which show a monotanic profile with heat flux approaching infinity near the leading edge. Clearly, a power law predicted by boundary layer theory, which neglects streamwise diffusion, can not fit the entire curve predicted by the numerical solutions given here. However, the right arm of the heat feedback curve may be fitted to a power law with an exponent of -0.7, which is also different from the boundary layer prediction of -0.5. Integration of the heat feedback curve shows that 70% of the total heat feedback from the flame is received by first 3 cm of the plate from the leading edge. This underscores the importance of the leading edge in accurate calculations of the heat feedback. This is crucial for burning of solids since heat feedback is the central driving mechanism for solid pyrolysis and heat transport. The numerical solutions presented here can predict the heat feedback on the entire surface that includes both the leading edge and boundary layer limits for a porous plate burner with well-defined solid boundary and for which accurate experimental data may be available for future comparisons.

7.0   ACKNOWLEDGMENTS

8.0 REFERENCES

Ananth, R., Ndubizu, C.C., Tatem, P.A., Patnaik, G., and Kailasanath, K., "A Numerical Model for Suppression of a Burning Solid Surface in Boundary Layer Flow", Proceedings of the 44 th International SAMPE Symposium and Exhibition, pages 1395-1407, Volume 44, Book 2, Evolving And Revolutionary Technologies for the New Millenium, Edited by Dr Leslie Jay Cohen, Jerome L. Bauer, William E Davis, Long Beach Convention center, Long Beach, California, May 23-27, 1999

Ananth, R., Ndubizu, C.C., Tatem, P.A., Patnaik, G., and Kailasanath, K., "Gas Phase Suppression of a Diffusion Flame Formed Over a Porous Solid Surface", Eigth International Conference on Numerical Combustion, Society of Industrial and Applied Mathematics (SIAM), Amelia, FL, March 5-8, 2000

Andreussi, P. and Petarca, L., "Film Combustion of Ethyl Alchol in a Parallel Air Stream", Eighteenth Symp. (International) on Combustion, The Combustion Institute, Pittsburgh, 1861(1981)Emmons, H.W., "The Film Combustion of Liquid Fuel", Z. Angew. Math. Mech., 36, 60(1956)

Brahmi, L., Vietoris, T., Joulain, P., David, L., and Torero, J.L., "The Effect of   Fuel Injection on a Laminar Diffusion Flame Established on Perpendicular Fuel and Oxidizer Streams", Submitted to Combustion and Flame, January 1999.

Burden, R.L. and Faires, J.D., "Numerical Ananlysis", PWS Publishers, Boston, 3 rd edition, (1985)

Casulli, V. and Greenspan, D., "Pressure Method for the Numerical Solution of Transient, Compressible Fluid Flows", International Journal for Numerical Methods in Fluids, 4, 1001(1984)

Chen, C-H. and Tien, J., "Diffusion Flame Stabilized at the Leading Edge of a Fuel Plate", Comb. Sci. and Tech., 50, 283(1986)

DeVore, C.R., "Vectorization and Implementation of an Efficient Multigrid Algorithm for the Solution of Elliptic Partial Diefferential Equations, NRL Memorandum Report 5504, Naval Research Laboratory, Washington DC (1984)

Ha, S.J., Shim, H.S., and Shin, D.H., "Boundary Layer Diffusion Flame Over a Flat Plate in the Presence and Absence of Flow Separation", Combust. Sci. and Tech., 75, 241(1991)

Hirano, T. and Kanno, Y., "Aerodynamic and Thermal Structures of the Laminar Boundary Layer Over a Flat Plate with a Diffusion Flame", Fourteenth Symp. (International) on Combustion, The Combustion Institute, Pittsburgh, 391(1973)

Kikkawa, S. and Yoshikawa, K., "Theoretical Investigation on Laminar Boundary Layer with Combustion on a Flat Plate", Int. Heat Mass Transfer, 16, 1215(1973)

Kodama, H., Miyasaka, K., and Fernandez-Pello, A.C., "Extinction and Stabilization of a Diffusion Flame on a Flat Combustible Surface with Emphasis on Thermal Controlling Mechanisms", Combust. Sci. and Tech., **54**, 37(1987)

Lavid, M. and Berlad, A.L., "Gravitaional Effects on Chemically Reacting Laminar Boundary Layer Flows Over a Horizontal Flat Plate", Sixteenth Symp. (International) on Combustion, The Combustion Institute, Pittsburgh, 1557(1976)

Mao, C.-P., Kodama, H., and Fernandez-Pello, A.C., "Convective Structure of a Diffusion Flame Over a Flat Combustible Surface", Comb. & Flame, **57**, 209(1984)

Oran, E.S. and Boris, J.P., "Numerical Simulation of Reactive Flow", Elsevier Publishing Co., New York, (1987)

Pagni, P.J., "Diffusion Flame Analyses", Fire Safety J, **3**, 273(1980)

Patnaik, G., Laskey, K.J., Kailasanath, K., Oran, E.S., and Brun, T.A., "FLIC-A Detailed, Two-Dimensional Flame Model", NRL Memorandum Report 6555, Naval Research Laboratory, Washington, DC, September 27, (1989)

Patnaik, G., Guirguis, R.H., Boris, J.P., and Oran, E.S., "A Barely Implicit Correction for Flux-Corrected Transport", NRL Memorandum Report 5855, Naval Research Laboratory, Washington, DC, September 30, (1986)

Penner, S.S., "Chemistry Problems in Jet Propulsion", Pergamon Press, Ney York, (1957)

Press, W.H., Flannery, B.P., Teukolsky, S.A., and Vetterling, W.T., "Numerical Recipes", Cambridge University Press, Cambridge, (1986)

Ramachandra, A. and Raghunandan, B.N., "An Analysis of a Boundary Layer Diffusion Flame Over a Porous Flat Plate in a Confined Flow", Combust. Sci. and Tech., **38**, 59(1984)

Ramachandra, A. and Raghunandan, B.N., "On the Velocity Overshoot in a Laminar Boundary Layer Diffusion Flame", Combust. Sci. and Tech., **33**, 309(1983)